Weather and Climate Extremes 34 (2021) 100402

Contents lists available at ScienceDirect

Weather and Climate Extremes

journal homepage: www.elsevier.com/locate/wace

Multi-type assessment of global droughts and teleconnections

Zahir Nikraftar [a], Abdorrahman Mostafaie [b,*], Mojtaba Sadegh [c], Javad Hatami Afkueieh [d], Biswajeet Pradhan [e,f,g,**]

[a] School of Surveying and Geospatial Engineering, College of Engineering, University of Tehran, Iran
[b] Surveying Department, Faculty of Engineering, University of Zabol, Zabol, Iran
[c] Department of Civil Engineering, Boise State University, ID, USA
[d] Department of Mechanics and Mechatronics, Academy of Engineering, Peoples' Friendship University of Russia (RUDN University), 117198, Moscow, Russia
[e] Centre for Advanced Modelling and Geospatial Information Systems (CAMGIS), School of Civil and Environmental Engineering, Faculty of Engineering and IT, University of Technology, Sydney, NSW, 2007, Australia
[f] Center of Excellence for Climate Change Research, King Abdulaziz University, P. O. Box 80234, Jeddah, 21589, Saudi Arabia
[g] Earth Observation Centre, Institute of Climate Change, Universiti Kebangsaan Malaysia, 43600, UKM, Bangi, Selangor, Malaysia

ARTICLE INFO

Keywords:
Combined standardized drought index (CSDI)
Terrestrial water storage (TWS)
NDVI
Vine copula
Drought index
Teleconnections

ABSTRACT

Several drought indices have been developed based on various processes (e.g., precipitation, soil moisture, vegetation health) that respond differently to modes of climate variability, shadowing their relatability to teleconnections, which in turn, limits drought forecasting. In this study, we advanced the multivariate analysis of droughts by using long-term Terrestrial Water Storage estimates, soil moisture and precipitation data along with normalized difference vegetation index. To this end, we employed a Vine copula approach using Archimedean and Elliptical copula families to generate two novel multivariate drought indices called Combined Standardized Drought Index (CSDI), based on agricultural, meteorological, hydrological and ecological univariate indices (i.e., the Eco-meteo-hydrologic index and the Agro-meteo-hydrologic index) for 33 major river basins across the globe between 1982 and 2015. To overcome the challenges associated with vine copula building blocks, we exhausted the possible choices of vine trees and selected the superior model based on a variety of performance metrics. CSDIs showed an integrated representation of univariate drought indices and revealed a more comprehensive and improved picture of intensity, duration and frequency of droughts. Our composite analysis showed that El Niño and La Niña have a significant impact on the regional drought occurrences across the globe, with highest impacts observed for fall. Results also showed that CSDIs can extract more conclusive anomalies in response to ENSO signals than univariate indices, as they better represent the ecosystem response to teleconnections.

1. Introduction

Various definitions of drought have been widely explored in the literature, including meteorological, hydrological, agricultural and socioeconomic droughts (Wilhite and Glantz, 1985; American Meteorological Society, 2004; Sadegh et al., 2017a; Jiao et al., 2019). The drivers of feedback between various drought periods are schematically presented in Fig. 1.

Using drought indices is a relatively simple way of quantitatively investigating and characterizing drought levels. Based on their foundational variables (e.g., precipitation, soil moisture, evapotranspiration), these indices represent different events and conditions within the region studied (Zargar et al., 2011). To extend traditional univariate drought indices, different statistical methods have been used to combine various aspects of droughts (Dikshit and Pradhan, 2021). Examples include copula functions (Kao and Govindaraju, 2010a,b; Mirabbasi et al., 2013; Kavianpour et al., 2018); principal component analysis (Abdi et al., 2017; Bazrafshan et al., 2014, 2015; Chang et al., 2016; Keyantash and Dracup, 2004; Waseem et al., 2015); entropy-based methods (Rajsekhar et al., 2015); variance-based approach (Murthy

* Corresponding author.
** Corresponding author. Centre for Advanced Modelling and Geospatial Information Systems (CAMGIS), School of Civil and Environmental Engineering, Faculty of Engineering and IT, University of Technology, Sydney, NSW, 2007, Australia.
E-mail addresses: nikraftarz@gmail.com (Z. Nikraftar), a.mostafaie@uoz.ac.ir (A. Mostafaie), mojtabasadegh@boisestate.edu (M. Sadegh), khatamiafkuiekh-d@rudn.ru (J.H. Afkueieh), Biswajeet.Pradhan@uts.edu.au (B. Pradhan).

https://doi.org/10.1016/j.wace.2021.100402
Received 11 May 2021; Received in revised form 5 October 2021; Accepted 29 November 2021
Available online 3 December 2021

et al., 2017) and the empirical weighting method (Balint et al., 2013). Among these approaches, copulas have been given much attention due to their parsimonious functional structure, flexibility, robustness and their ability to merge univariate distributions of different forms (Sadegh et al., 2017b). A prominent example among several such applications is that of Hao and AghaKouchak (2013), Ma et al. (2015), Rad et al. (2017), Yang et al. (2018) and Zhang et al. (2017) which characterized meteorological and agricultural drought conditions. They developed a Multivariate Standardized Drought Index (MSDI) by combining Standardized Precipitation Index (SPI) and Standardized Soil Moisture Index (SSI), using copula functions and showing that by using MSDI, the detected drought onset is almost the same as that of SPI, while the duration of the drought is more similar to SSI behavior.

This study develops two copula-based CSDIs: the $CSDI^1$ is constructed from the combination of meteorological drought (SPI), hydrological drought (Standardized Water Storage Index), (SWSI) and ecological drought (Standardized Vegetation Index), (SVI) indices, and the $CSDI^2$ is constructed from the combination of meteorological drought (SPI), hydrological drought (SWSI) and agricultural drought (Standardized Soilmoisture Index), (SSI) indices. We compute univariate (SPI, SWSI, SSI and SVI) and the proposed combined drought indices (i.e., $CSDI^1$ and $CSDI^2$) for the world's 33 major river basins – as defined by the Global Runoff Data Centre (see Fig. 2). The developed CSDIs for each basin reflect hydro-eco-meteorological drought evolutions and hydro-agri-meteorological drought evolutions.

We then explore the impacts of the El Ni ñ o Southern Oscillation (ENSO) – as the most prominent mode of globally-interconnected climate variability (Yeh et al., 2018) – on ecological, agricultural, meteorological and hydrological droughts, along with their joint distributions ($CSDI^1$ and $CSDI^2$), using a composite analysis method. We describe how these indices are affected by ENSO events. Many studies showed that ENSO has a significant influence on seasonal precipitation and temperature patterns across various regions of the globe (Dai and Wigley, 2000; Davey et al., 2014; Kiladis and Diaz, 1989; Ropelewski and Halpert, 1987; Tamaddun et al., 2019; Trenberth et al., 1998; Yang and Delsole, 2012). There are strong links between ENSO and drought conditions across the different regions of the world.

The major contributions of this study involve: **(A)** providing novel and significant insights relating to global-scale univariate and multivariate drought evolution, focusing on ecological, agricultural, hydrological and meteorological droughts simultaneously, **(B)** analyzing the best copula functions in a trivariate Vine copula framework for 33 of the largest basins in the world, and **(C)** evaluating and discussing the performance of the CSDIs to analyze the effect of teleconnection on drought conditions worldwide between 1982 and 2016. To overcome the challenges associated with vine copula building blocks, we exhausted the possible choices of vine trees and selected the superior model based on a variety of performance metrics. The novelties of this study are as follows. A nuanced, improved understanding of the impacts of univariate index selection on multivariate drought analysis within the vine copula modeling framework. Incorporation of the impacts of anthropogenic activities in drought analysis, using irrigation-induced soil moisture proxy, and development of trivariate drought indices that improve ecological and agricultural drought analysis. Improved understanding of teleconnection impacts on drought onset, development and termination, as demonstrated through a composite analysis of El Nino and La Nina phenomena and multivariate drought indices. Comprehensive investigation of the performance of multivariate indices in capturing the effect of ENSO on global ecosystem response as compared to univariate indices.

The remainder of the paper is organized as follows. In section 2, a general overview of the data used in this study is presented. Section 3 presents the methodology used to calculate univariate and proposed multivariate drought indices. In section 4, the results are analyzed and interpreted, and in section 5 a discussion is presented and section 6 concludes the paper.

2. Data

2.1. TWS estimates from GRACE

TWS estimates from the latest release of GRACE level two (L2) products that represent monthly gravity field solutions during 2003–2016 were used in this study (available at http://www2.csr.utexas.edu/grace/). To calculate the TWS time series, in accordance with Wahr et al. (1998), GRACE level two data were converted to smoothed fields by means of four steps: 1- Replacing degree 1 coefficients by those of Swenson et al. (2008); 2- Replacing degree 2 and order 0 coefficients by the more stable estimations of Chen et al. (2007); 3- Reducing anomalies due to the Glacial Isostatic Adjustment (GIA), using the output of the model provided by Geruo et al. (2013) and 4- Applying the DDK2 anisotropic filter (Kusche et al., 2009) to reduce the correlated noise in L2 products.

The study of droughts requires time series that span a climatic period – e.g., 30 years. The limitation of GRACE data in drought monitoring applications (i.e., short operational time) is mitigated hereby, extending the GRACE TWS time series back to 1980. Following Forootan et al. (2019), the W3RA model of van Dijk (2010) was used to extend the TWS estimates through estimation of a scale factor and a bias (vertical shift), and to match the long-term W3RA TWS to that of GRACE common data.

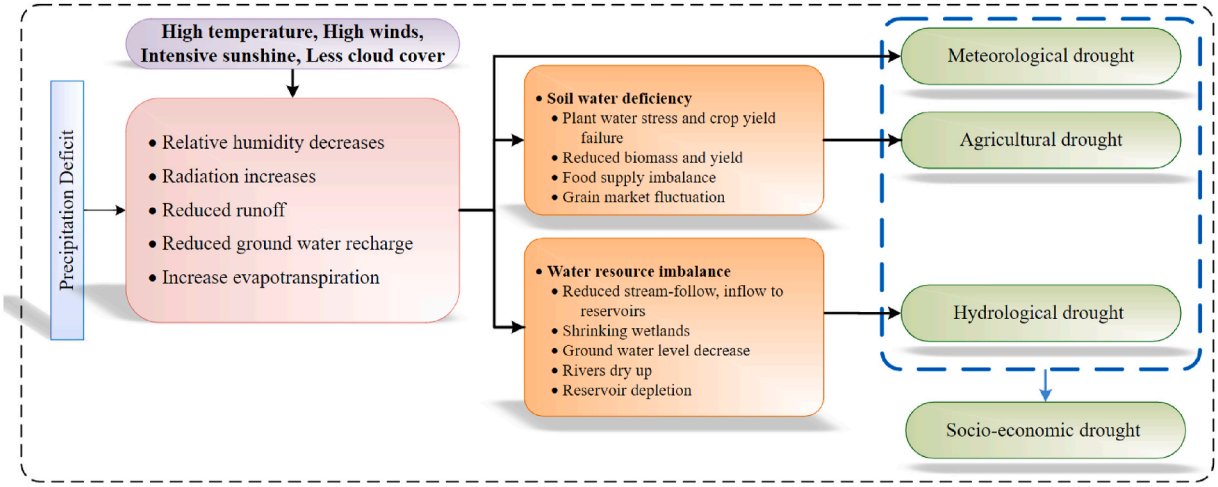

Fig. 1. Various drought types, their drivers and interactions.

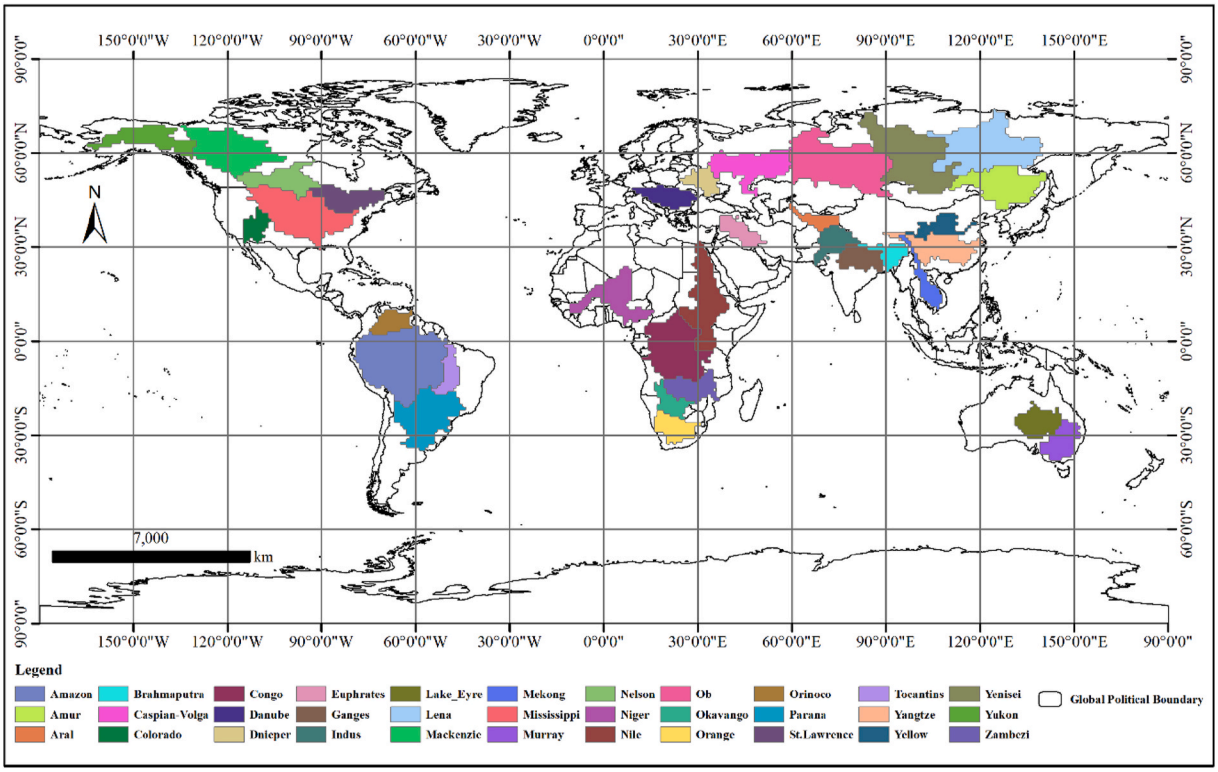

Fig. 2. The world's 33 major river basins were analyzed in this study.

The extended TWS time series of 1980–2016 was then applied to compute SWSI.

2.2. Global soil moisture and precipitation products

Precipitation and soil moisture data from the Modern-Era Retrospective Analysis for Research and Applications (MERRA) re-analysis are used in this study. The MERRA data span the period from 1979 to February 2016 and provides hourly total surface precipitation and soil moisture at a $0.5^\circ \times 0.67^\circ$ resolution. Interested readers are referred to Rienecker et al. (2011) for a brief overview of this dataset and discussion on its accuracy. In the current study, monthly precipitation (total surface precipitation) and soil moisture (total profile soil moisture content) from MERRA Land (provided by Aghakouchak and Nakhjiri (2012), http://amir.eng.uci.edu/data.php) averaged across the study basins, have been used to compute SPI and SSI drought indicators.

2.3. Normalized difference vegetation index (NDVI)

NDVI (Rouse Jr. et al., 1974), uses visible and near-infrared bands of the electromagnetic spectrum to provide a simple indicator of vegetation health. NDVI is widely used for ecological drought monitoring and has also been used for agricultural drought analysis. One of the early studies to demonstrate the value of NDVI in drought monitoring was that of Tucker et al. (2005) which applied a time-series of Advanced Very High-Resolution Radiometer (AVHRR) NDVI observations to characterize the drought of the early 1980s across the African Sahel region. In this study, a monthly composite of NDVI3g data with a spatial resolution of 8-km were used to calculate SVI, which is an NDVI-based drought index.

3. Methodology

Drought indices are numerical value representations of drought conditions. More than 150 drought indices have been developed and used for the assessment of this natural phenomenon (Zargar et al., 2011). Generally, these indices could be divided into two main groups, namely univariate and multivariate indices. Univariate indices are derived from one indicator and usually characterize only one type of drought; however, multivariate indices can inform a simultaneous evaluation of different types of droughts.

We have elected precipitation, terrestrial water storage, normalized difference vegetation index and soil moisture as a comprehensive list of drought-related available variables for this analysis. While we can expand this list, they will offer redundant information, as the studied variables already capture various ecosystem responses to lack of water. While univariate analysis with an extended set of variables is possible, by incorporating redundant information in the multivariate analysis, we may introduce a bias toward a certain process while discounting the impact of another.

Given the precipitation and agricultural activity gradients in various basins, we opted to analyze droughts at the basin scale. Specifically, there is a disproportionately higher precipitation in the high elevations, whereas the majority of the agriculture occurs in the lower elevations of various basins. Our analysis allows for incorporation of using streamflow as a source of irrigation. Although grid-based drought analysis is widely explored in the literature but considering precipitation and NDVI at the catchment level will allow to account for interrelationship between these factors and irrigation, while using grid-based analysis might induce an underestimation of hydrological drought impacts on agriculture. In the following sub-sections, the univariate indices, used in this study, are described, and the calculation of two novel trivariate indices (i.e., NDVI-SPI-SWSI and SSI-SPI-SWSI) using copula functions, is explained.

3.1. Univariate drought indices

The concept of drought is region-specific, given that precipitation varies significantly across various regions of the world. The World Meteorological Organization (WMO) suggests that all national meteo-

rological and hydrological services use SPI to achieve comparable drought analysis on a global scale. The same description that was used for SPI, based on precipitation, can be applied to soil moisture, water storage anomaly and NDVI, to calculate associated drought indices. The calculation of SPI and other drought indices involves fitting certain distributions to the observed data. However, due to the difference in climatic conditions, different hydrological or meteorological variables can have wildly different probability distributions (Farahmand and AghaKouchak, 2015). Therefore, using a parametric approach (i.e., fitting distributions) to calculate standardized drought indices, could lead to inconsistent results from one region to another. To alleviate this shortcoming, Farahmand and AghaKouchak (2015) presented a generalized framework based on non-parametric measures to provide statistically consistent and comparable drought indices. Using this framework, a nonparametric standardized index can be calculated, using the empirical probability of univariate indices instead of the gamma (or any other parametric) distribution function. The empirical Gringorten plotting position (Equation. 1) was used in this study to derive the univariate probability of different variables (Gringorten, 1963):

$$p(x_i) = \frac{i - 0.44}{n + 0.12} \tag{1}$$

where, i is the rank of the ith observed value, starting from the smallest observation and n is the number of observations. The probabilities derived from Equation (1) could be transformed into a Standardized Index (SI) by applying the inverse of a standard normal distribution function (Equation (2)).

$$SI = \varphi^{-1}(p) \tag{2}$$

where φ and p are the standard normal distribution function and the probability value from Equation (1), respectively.

In this study, monthly precipitation, soil moisture, NDVI and total water storage data are used to estimate three- and 12-month SPI, SSI, SVI and SWSI. SPI exhibits the departure of precipitation from its long-term average at a specific temporal scale (Bayissa et al., 2018). SSI utilizes the z-score to explain the deviation of soil moisture from the historical mean (AghaKouchak, 2014). The SVI is based on vegetation conditions and informs on agricultural and ecological droughts (Zargar et al., 2011). SWSI is an indicator, based on TWS observations, which reflects the properties of hydrological drought (Zhu et al., 2018).

3.2. CSDI using copula

Copulas can be used to construct a multidimensional distribution from uniform marginals (Sklar, 1959). Copulas have the ability to couple multiple random variables with any given dependence structure, regardless of their univariate probability distribution functions, and construct a dependent variable that contains all key characteristics of the independent indices. Sklar (1959) defined copula as:

$$F(x_1, \ldots, x_n) = C(F_1(x_1), \ldots, F_n(x_n)) = C(u_1, \ldots, u_n) \tag{3}$$

where c is the Copula function mapping $C : [0,1]^n \rightarrow [0,1]$ and f is the n-dimensional joint Cumulative Distribution Function (CDF) of a random vector of size n (i.e., $X = [x_1, \ldots, x_n]^T$) with marginal cumulative distributions of $F_1, \ldots, F_n$.

Four general families of copulas exist, including elliptical, Archimedean, extreme-value and certain other miscellaneous copulas. As suggested by Rad et al. (2017), the elliptical and Archimedean copulas are the best copulas for modelling multidimensional hydrological variables. In this study, six copula functions from the elliptical and Archimedean families are employed to construct a multidimensional CDF (Schepsmeier et al., 2018). The specifications of these copulas are listed in Table 1.

This study aims to investigate the advantages of the proposed CSDIs, ($CSDI^1$ and $CSDI^2$) by comparison with univariate indices. The $CSDI^1$ and $CSDI^2$ represent meteorological-hydrological-ecological and meteorological-hydrological-agricultural drought indices, respectively. These indices are composed of various univariate drought indices and combine the drought characteristics into two unified metrics, using the Vine copula approach (find more details relating to copula in the supplementary information). The CSDIs are calculated by means of three key steps which are shown in Fig. 3 and are briefly described in the following sections.

Step 1. Pre-processing

Data relating to the monthly basin-wide averages of precipitation, total water storage anomaly, soil moisture and NDVI are extracted for the 33 major basins of the globe, and SPI, SWSI, SSI and SVI are computed in two different time scales, i.e., three and 12 months (Dikshit et al., 2020a, b, 2021a, b). Short accumulation periods (e.g., three months) of SPI can be used as indicators of immediate impacts, such as reduced soil moisture, snowpack and flow in smaller basins (WMO, 2016). Medium accumulation periods (between three and 12 months) of SPI can be used as an indicator of reduced streamflow in medium-to large-sized watersheds and reservoirs. Finally, when SPI is computed for longer accumulation periods (e.g., 12 months or more), this can be used as an indicator for reduced reservoir and groundwater recharge. It should be noted that the relationship between the accumulation period and the drought impact is highly dependent on regional characteristics, such as soil structure and human intervention. Therefore, a comprehensive investigation of drought impacts can only be carried out when drought indices are compared across various accumulation periods. We consider three- and 12-month accumulation periods and note that our proposed framework is generic and can be used at various accumulation periods. Table S1 presents details relating to standardized drought categories.

Table 1
Characteristics of six different copula functions were used in this study.

Family	Name	Copula function	Variables
Archimedean	Gumbel	$C\left(u,v\right) = \exp\left\{ - \left(- \ln u\right) - \ln v)(-\ln v)(-\ln v)^{\theta}\right]^{\frac{1}{\theta}}\right\}; \theta \in [1, \infty)$	Bivariate
	Frank	$C(u,v) = -\frac{1}{\theta}\ln\left[1 + \frac{(e^{-\theta u} - 1)(e^{-\theta v} - 1)}{e^{-\theta} - 1}\right]; \theta \in \Re \backslash \{0\}$	Bivariate
	Clayton	$C\left(u,v\right) = (u^{-\theta} + v^{-\theta} - 1)^{-\frac{1}{\theta}}; \theta \in [-1, \infty)\Big\backslash \{0\}$	Bivariate
	Joe	$C(u,v) = 1 - 1 - u)1 - v)1 - u)1 - v)(1 - v)(1 - v)^{\theta}]^{1/\theta}; \theta \in [1, \infty)$	Bivariate
Elliptical	Gaussian	$C\left(u\right) = \frac{1}{\sqrt{\lvert R\rvert}}\exp\left[-\frac{1}{2}\begin{pmatrix}\varphi^{-1}(u_1)\\ \vdots \\ \varphi(u_n)\end{pmatrix}^{T}\left(R^{-1} - 1\right)\right]\begin{pmatrix}\varphi^{-1}(u_1)\\ \vdots \\ \varphi(u_n)\end{pmatrix}$	Multivariate
	t-student	$C(u) = \frac{f(F_1^{-1}(u_1), \ldots, F_p^{-1}(u_p))}{\prod_{i=1}^{p} f(F_i^{-1}(u_i))}$	Multivariate

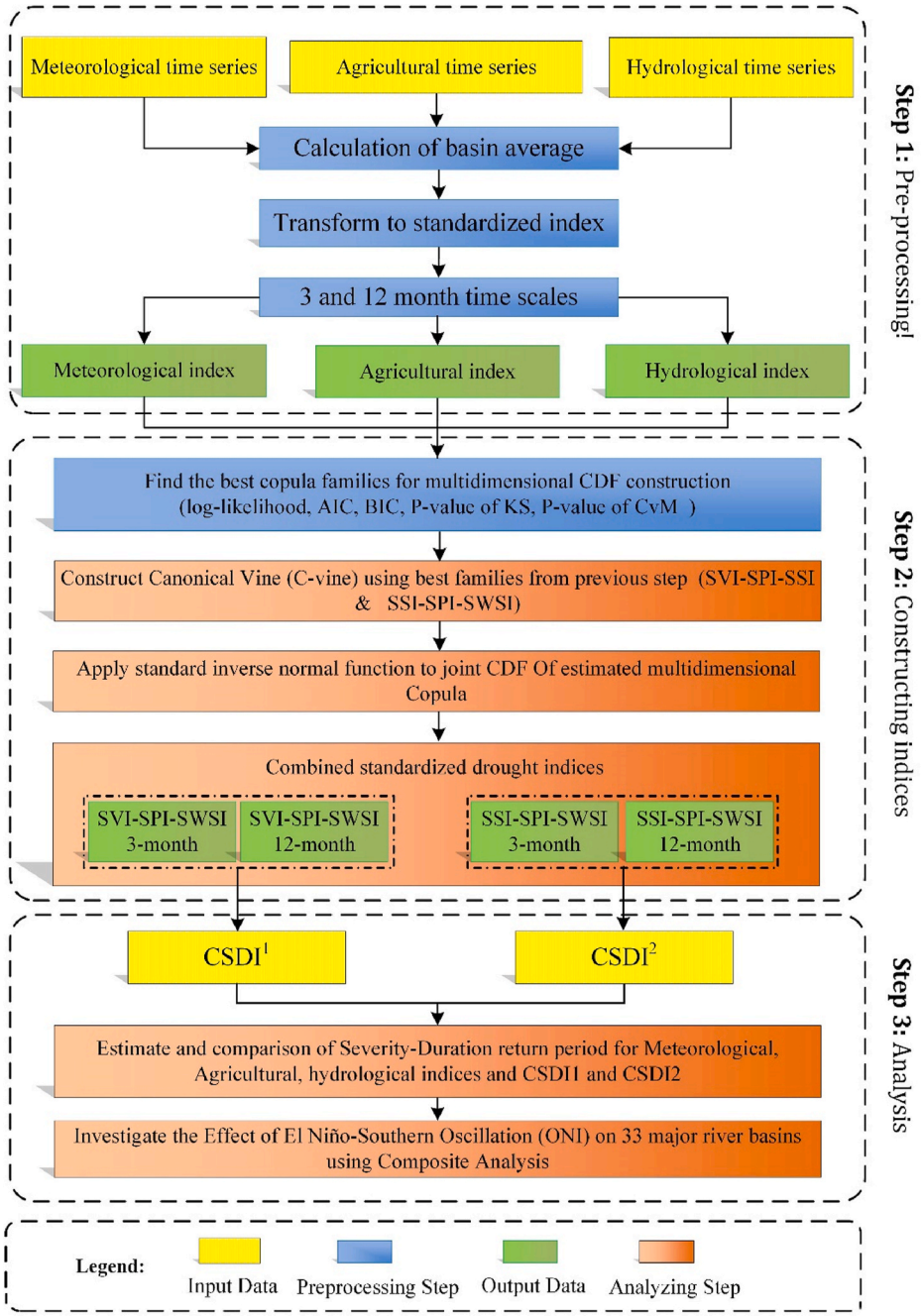

Fig. 3. Flowchart of the employed methodology to calculate CSDIs ($CSDI^1$ and $CSDI^2$).

Step 2. Constructing trivariate indices

CSDIs are calculated by means of a three-dimensional CDF, using nested bivariate copulas and univariate indices (i.e., SVI, SPI, SSI and SWSI). To construct the trivariate CSDIs, we exhaust all choices of combinations of the Archimedean and elliptical copula families. The Kolmogorov-Smirnov (K-S) and Cram e′ r-von Mises (CvM) tests, along with log-likelihood ratio and AIC and BIC criteria, are then used to investigate the performance of various constructs of trivariate copulas. K-S and CvM tests with p-values equal or higher than 0.05 (i.e., 5% significant level) show an acceptable constructed Vine copula (Kavianpour et al., 2018). The constructed Vine copula model with the highest values of log-likelihood and the lowest values of AIC and BIC represents the best model, which is, in turn, selected for drought analysis. Subsequently, CSDIs ($CSDI^1$ and $CSDI^2$) are calculated based on two different combinations of univariate indices for drought monitoring. The first trivariate index ($CSDI^1$) is calculated based on SVI-SPI-SWSI, and the second trivariate index ($CSDI^2$) is calculated based on SSI-SPI-SWSI. Both trivariate indices are calculated across three- and 12-month time scales. These two indices collectively, provide a certain insight into the human effects on drought, as SSI incorporates the irrigation and anthropogenic elements of drought, whereas the anthropogenic impacts on SVI are less pronounced.

Step 3. Analysis

The analysis Step consists of two sub-steps: firstly, estimating drought characteristics using the calculated indices and secondly, comparing the ENSO-related anomalies of drought indices.

Step 3-1. Estimate and compare the severity-duration-frequency curves of meteorological, agricultural, hydrological and CSDI drought indices

In this Step, the probability of drought occurrence events was calculated (involving SPI, SWSI, SSI, SVI and their combined behavior, CSDI[1], and CSDI[2]). The duration and severity can be determined directly from the variation in the SPI values.

- Drought duration (D) is defined as the number of consecutive months in which SPI remains equal to or below the 20th percentile threshold (McKee et al., 1993).
- Drought severity (S) is defined as the cumulated negative SPI values in drought duration D (Mellak and Souag-Gamane, 2020) and $S = -\sum_{i=1}^{D} SPI_i$, where SPI$i$ is the SPI value in the ith month (SPIi < 0).

Step 3-2. Comparison of ENSO-related anomalies of drought indices

The relationship between climate change and its effect on drought has been the focus of multiple studies in recent years, but given the complexities of drought, further and more detailed research is needed to fully understand the drivers of this reoccurring phenomenon (Wang et al., 2014). Trenberth et al. (2014) discuss that natural phenomena like ENSO are among the most important reasons for drought episodes, with major societal and economic repercussions. The National Centers for Environmental Prediction (NCEP) of National Oceanic and Atmospheric Administration (NOAA) uses the Oceanic Niño Index (ONI) as a standard metric for monitoring El Niño (warm) and La Niña (cool) events in the tropical Pacific. ONI is derived from a three-month running mean of Sea Surface Temperature (SST) anomalies across the Niño 3.4 region. The warm (El Niño) and cold (La Niña) phases of ENSO are defined as five consecutive months within which ONI indices pass the threshold of +0.5° (for El Niño) and −0.5° (for La Niña) events. The NCAR climate data guide has established four categories for El Niño events and three categories for La Niña events, based on the ONI index, which are demonstrated in Fig. 4 and summarized for the years 1982–2015 in Table 2. The years that are not mentioned in Table 2, are the non-ENSO events.

Harisuseno (2020) after investigating the performance of Standardized Precipitation Index and Percent of Normal Index using SOI index, they suggested that oceanic teleconnection could be used as a variable to verify the reliability of drought indices. Hence, in this study, the effects of ONI on SVI, SPI, SWSI and CSDI drought episodes are investigated, based on a composite analysis approach. Here, we use strong and very strong El Niño categories for constructing the El Niño composite and a strong La Niña category for constructing a La Niña composite. To analyze the effect of ENSO on global drought, composite analysis is applied to the March-April-May (MAM), June-July-August (JJA), September-October-November (SON) and December-January-February (DJF) seasons of each year. For each index at a three-month time scale, the Drought Composite Anomaly (DCA) of MAM, JJA, SON and DJF was calculated using Equation (4). A deviation of seasonal means of drought indices during El Niño/La Niña events from their normal condition (i.e., seasonal mean during a non-ENSO event) provides us with the drought anomalies tied to the ENSO phenomenon.

$$DCA = \text{mean}\,(X_{i\,\in\,ENSO}) - \text{mean}(X_{i\,\in\,non-ENSO}) \quad (4)$$

where x is the vector of drought indices in the aforementioned seasons and i represents years.

4. Results and discussion

4.1. Univariate drought indices

Drought indices are all standardized by design, which makes them comparable in the period of this study. Table S2 summarizes the results of cross-correlation analysis between the different indices of a three-month scale (SPI set as the reference index) that show conformity and discrepancies between these indices across different basins. Specifically, the maximum correlation coefficient between SPI and SWSI, SSI and SVI, are calculated by exploring various lag times. The results are summarized in Fig. 5, which shows that the maximum and minimum correlation of the SWSI index with SPI is 0.74 and 0.24, respectively. For most of the studied basins, there is a two-month lag between SPI and SWSI drought indices. SPI also shows a high level of correlation with SSI, with Pearson correlation coefficients that vary between a minimum of 0.21 and a maximum of 0.81. The average lag difference between SSI and SPI is also two months, varying from one to six months in various basins. In most basins, this lag is between one and three months, which shows that SSI does conform well to SPI. The correlations of basin average SVI and SPI are rather low in most basins, varying from a minimum of 0.08 and a maximum of 0.55. In most basins, there is a lag of two to four months between SPI and SVI. In general, the basin average of SVI shows a lower correlation level, compared to SWSI and SSI, with SPI.

Now that the correlation level among various drought indices has been established, we proceed to find the best copula families to construct a three-dimensional joint distribution. Archimedean, Elliptical and their combination have been used to construct the joint CDF for all basins, among which four basins, namely the Amazon, Mississippi, Nile and Niger are presented here. The best copula family is chosen, based on the K-S and CvM tests, as well as Akaike and Bayesian Information Criteria and log-likelihood measure. Test results are listed in Table S3, showing that joint distributions, constructed by a combination of Archimedean and Elliptical copula families, have higher values of log-likelihood and lower values of AIC and BIC, pointing to their superior performance. The K-S and CvM tests show p-values greater than the 0.05 for all basins and all contributed families, implying they are all admissible (cannot be rejected).

Goodness-of-fit results for the constructed CSDIs, using Vine copula (K-S and CvM test P-value and their statistics, AIC, BIC and Log-Likelihood) are listed in Tables S4 and S5 across a three-month time scale. For the first scenario (SVI-SPI-SWSI; Table S4), mostly SPI and SWSI have been chosen as a conditional index to form the second tree of the Vine copula. For the second scenario (SSI-SPI-SWSI; Tables S5) and

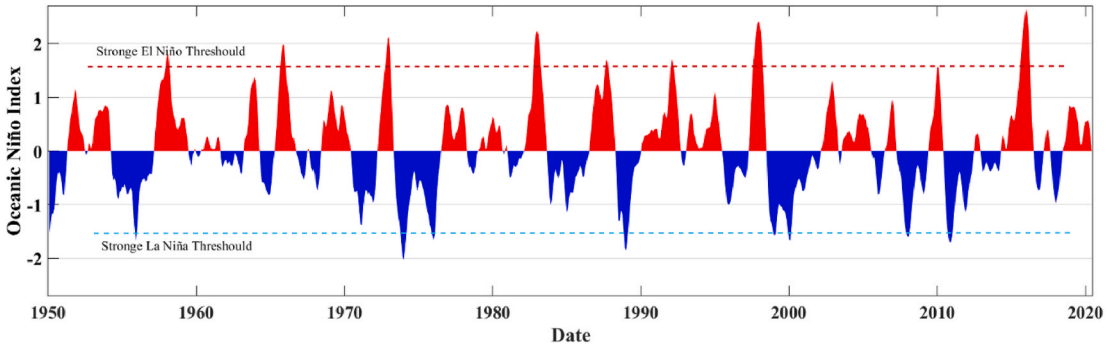

Fig. 4. ONI time series from 1950 to 2020. Red shaded areas demonstrate El Niño events and blue shaded regions demonstrate La Niña events.

Table 2
ENSO events categories.

El Niño				La Niña		
Weak	Moderate	Strong	Very Strong	Weak	Moderate	Strong
2004–05	1986–87	1987–88	1982–83	1983–84	1995–96	1988–89
2006–07	1994–95	1991–92	1997–98	1984–85	2011–12	1998–99
2014–15	2002–03		2015–16	2000–01		1999–00
	2009–10			2005–06		2007–08
				2008–09		2010–11

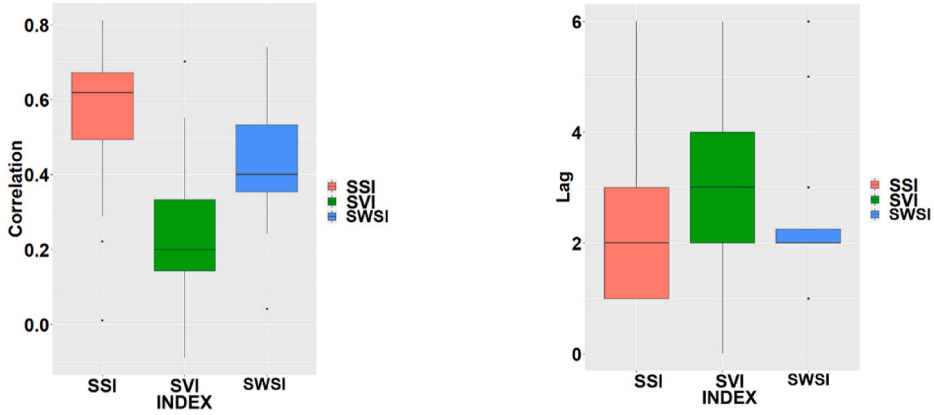

Fig. 5. Boxplot of maximum correlation (left) and its associated lag (right) in the months between SPI versus SSI, SVI and SWSI for the basins studied.

SSI has been chosen as the conditional index in the majority of basins. For both scenarios in all basins, the K-S and CvM test p-values imply that the constructed Vine copula cannot be rejected at a significance level of 0.05. Values of AIC and BIC for the second scenario (SSI-SPI-SWSI) are significantly smaller than for the first scenario (SVI-SPI-SWSI), which indicates that the construction of the Vine copula, based on SSI shows a better goodness-of-fit than that of SVI. Also, the values of log-likelihood for the second scenario are much greater than the first, attesting to the validity of this claim. By comparing the correlation values for the SVI in Table S2, versus log-likelihood values in Table S4, it is evident that the performance of the 3D-Vine for the basins with the statistically insignificant correlation between vegetation index (SVI) and other indices, deteriorates significantly. This is demonstrated in Fig. 6 a, which shows the scatter plot of an SPI-SVI correlation value (see the value of the X-axis in Fig. 6a) and log-likelihood (higher value of log-likelihood shows better goodness-of-fit). In the second scenario (SSI-SPI-SWSI), there is a positive correlation between SPI and SSI (see the value of the X-axis in Fig. 6b) and also values of log-likelihood are much higher by comparison with the first scenario. The scatter plot of SPI-SSI correlation and log-likelihood for the second scenario is demonstrated in Fig. 6 b.

Plots of empirical probabilities against Vine copula simulated probabilities (Fig. 7) also attest to the sufficiency of the 3-D joint probability models for the Amazon, Mississippi, Nile and Niger basins. Indeed, this figure shows that no significant difference between empirical and modelled joint probabilities can be detected. The results of the K-S test, comparing the empirical and Vine copula-simulated CDF of the Amazon, Mississippi, Niger and Nile are listed in Table 3. P-values for both scenarios (SVI-SPI-SWSI and SSI-SPI-SWSI) are greater than the 0.05 significance level, which shows that the empirical and modelled CDF share the same underlying distribution. P-values of the second scenario (SSI-SPI-SWSI) are much greater than the P-values of the first scenario (SVI-SPI-SWSI), once again confirming that the Vine copula model for the second scenario, performed better than the first scenario.

4.2. CSDI

Drought characteristics such as duration, severity, intensity, onset and persistency could be different in various drought indices. For example, hydrological indices, such as the water storage drought index, indicate a higher persistence of the drought condition as compared to the meteorological drought, given that temporal fluctuations of river flow or water storage are very gradual compared to precipitation. In the case of the SVI, vegetation could also exhibit a significant lag in response to a lack of precipitation. The relationship between meteorological,

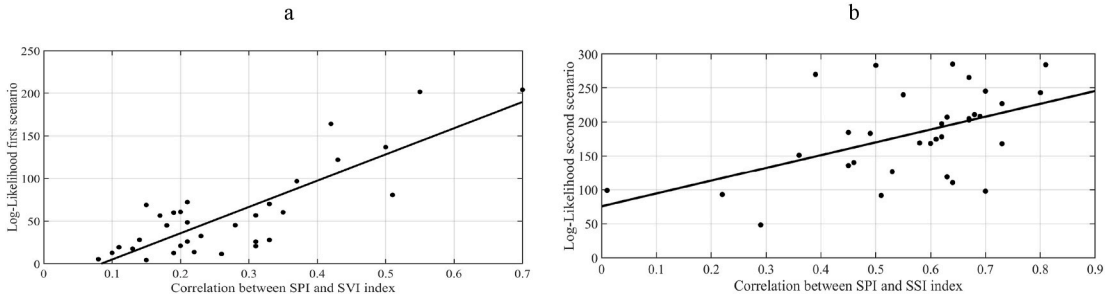

Fig. 6. Scatter plots of a) SVI-SPI correlation and log-likelihood of the first scenario (SVI-SPI-SWSI) and b) SSI-SPI correlation and log-likelihood of the second scenario (SSI-SPI-SWSI).

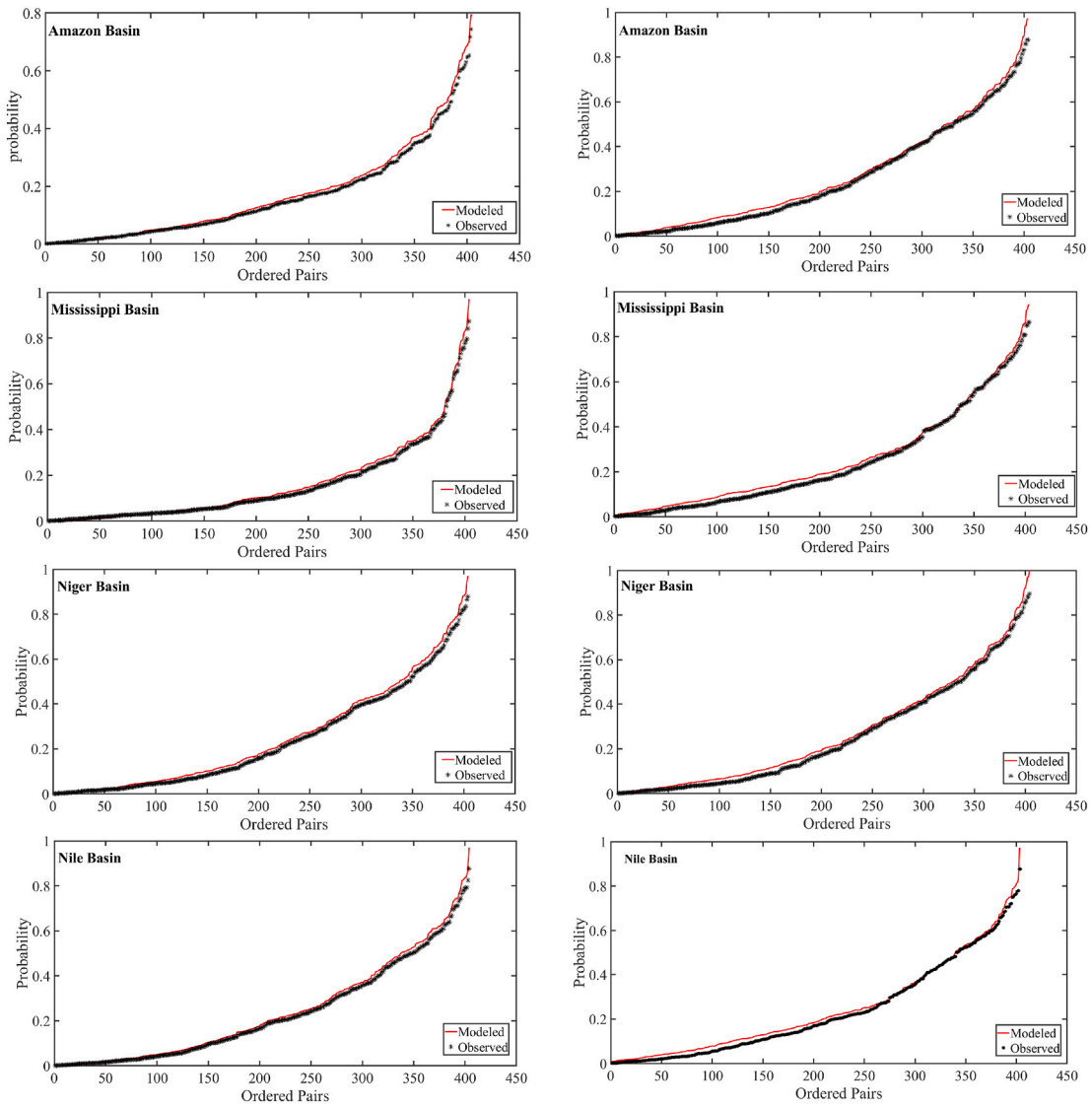

Fig. 7. Comparison of empirical probabilities (i.e., observed probability) versus Vine copula-modelled joint distribution for the CSDI[1] (left column) and the CSDI[2] (right column) for the Amazon, Mississippi, Niger and Nile basins.

Table 3
K-S test results measuring the distance between empirical and modelled CDF for the four selected basins.

	SVI-SPI-SWSI		SSI-SPI-SWSI	
Basin	P-value	K-S statistic	P-value	K-S statistic
Amazon	0.15	0.07	0.85	0.04
Mississippi	0.10	0.08	0.63	0.05
Niger	0.09	0.09	0.57	0.05
Nile	0.12	0.08	0.85	0.04

agricultural and hydrological droughts is very complex, which makes the behavior of CSDIs very intricate. The expectation from the CSDIs is to provide a new comprehensive perspective of drought, which stems from the joint probability distribution of precipitation, groundwater and soil moisture or vegetation. The performance and characteristics of the CSDI[1] and CSDI[2] are investigated here and described in the following paragraph, with a detailed example over the Mississippi basin.

The time series of the CSDI[1] and CSDI[2] along with their univariate indices for the three- and 12- month time scales are presented in Fig. 8 and Fig. 9 over the Mississippi basin. Short-term fluctuations in drought conditions are more common at the three-month time scale, indicating that this is an accurate accumulation scale for early warning and management for agricultural purposes. Long-term drought is better represented at the 12-month time scale. Hence, we investigate the behavior of the CSDIs at both time scales (three months and 12 months) to analyze the characteristics of this novel drought index for short and long droughts. It has been noted that CSDIs indicate the severity based on the state of all univariate indices; hence, CSDIs can represent an even more severe situation compared to each univariate drought index. For example, for the 2013 and 2015 droughts in Fig. 8 a and the 1988 drought in Fig. 8 b, CSDIs indicate a more severe drought compared to univariate indices. This characterizes the compounding effects of various drought types (Sadegh et al., 2018). In the case that univariate indices present different severities, CSDIs represent the temporal severity, based on the drought state of all indices (for example the 1984, 1989, 1996, 2006 and 2010 droughts in Fig. 8 a and the 1989, 1996, 2006 and 2013 droughts in Fig. 8b). This represents the condition that one driver (e.g., precipitation) is in a deficit state, however, the normal or surplus conditions of other drivers(s) (e.g., total water storage) can alleviate the impacts of the deficit in the former driver. From Fig. 9 a, it has been noted that during the 1987–1988 drought, SWSI captures the drought condition later than SPI and earlier than SVI. Moreover, SPI returns to the normal condition sooner than other indices, as other

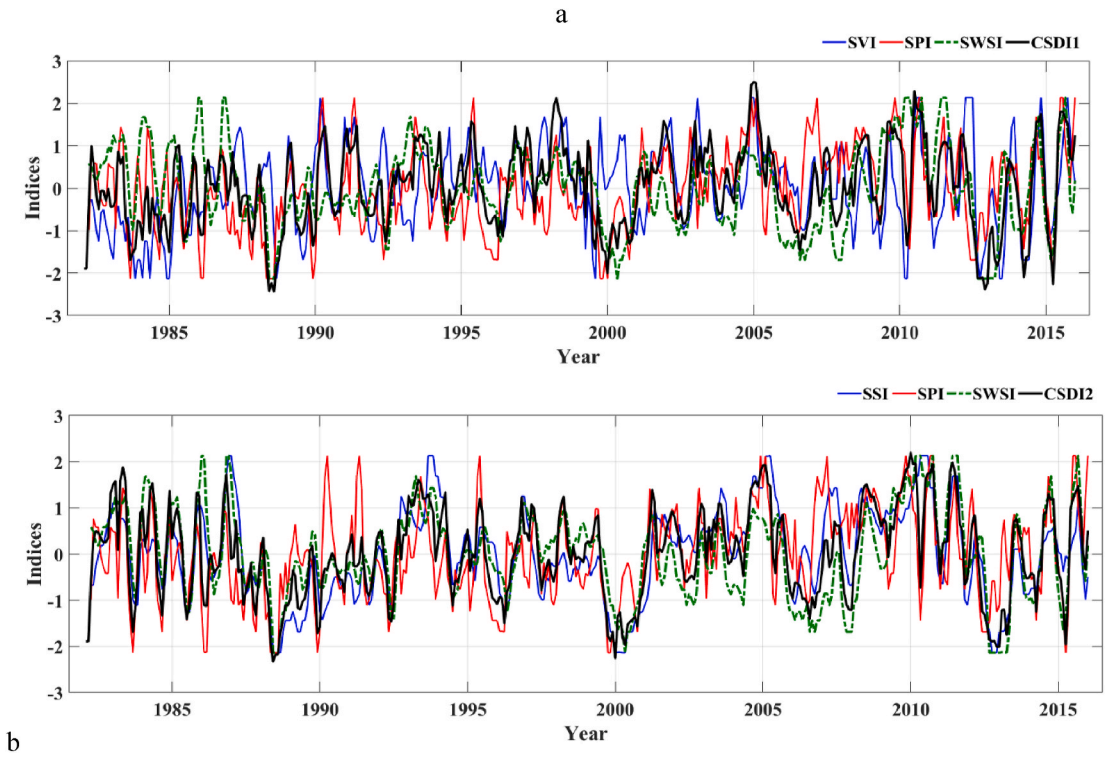

Fig. 8. Time series of a) SVI, SPI, SWSI, CSDI[1] and b) SSI, SPI, SWSI, CSDI[2] at the three-month time scale for the Mississippi basin.

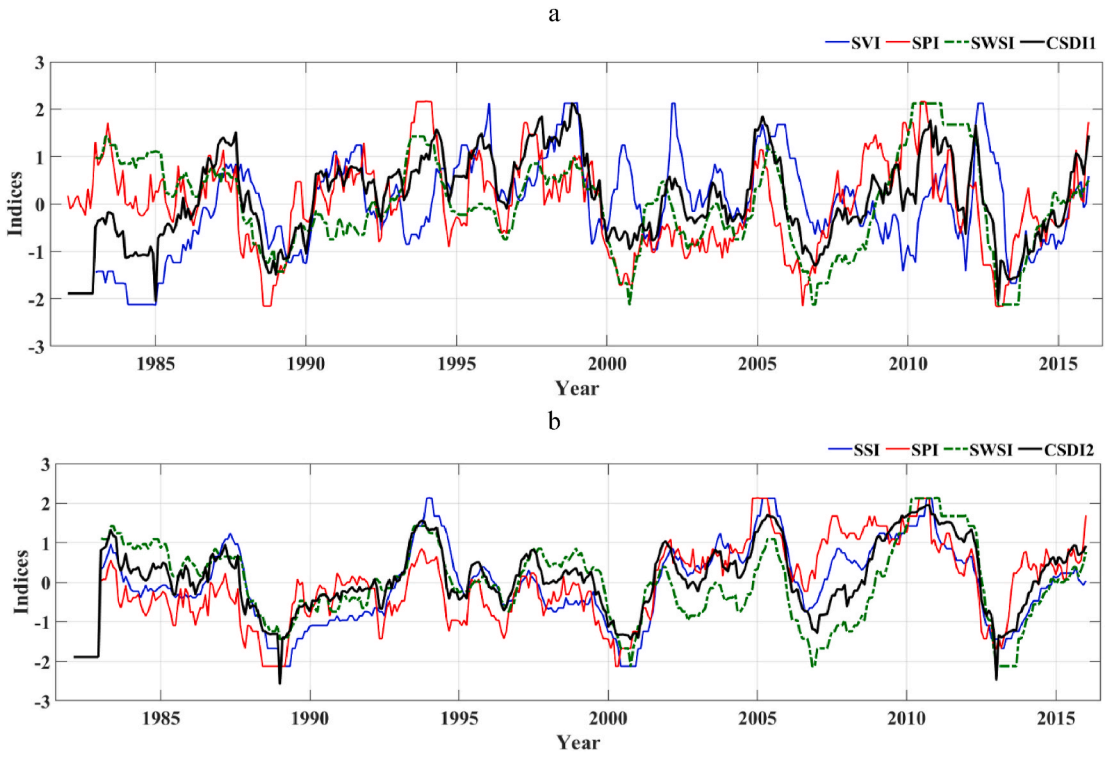

Fig. 9. Time series of a) SVI, SPI, SWSI, CSDI[1] and b) SSI, SPI, SWSI, CSDI[2] at the 12-month time scale for the Mississippi basin.

variables respond to precipitation. The CSDI[1] captures the drought onset, similar to SWSI and returns to normal conditions (drought termination) similar to SVI. For example, in Fig. 8 a, in the 2012 drought, the CSDI[1] captures the onset of drought similar to SWSI (SWSI captures the drought onset after SPI and earlier than SVI) and remains in a drought condition for a longer period than SPI and a shorter period

than SVI. Similar behavior is observed at the 12-month scale droughts of 1999 and 2006 in Fig. 9 a.

The SPI and SSI are generally consistent, but SSI's response to precipitation is a little slower compared to SPI. For example, in the 1989, 2006 and 2013 droughts, SSI remains in drought conditions longer than SPI (Fig. 9b). This behavior could be due to several reasons, including abnormally high precipitation over a short period. In this situation, most of the month remains dry, leading to SSI <0, whereas a few intense precipitation events drive SPI to a normal condition. This is yet another reason why describing the drought state, based on one index, could lead to a misinterpretation of the real drought state. Furthermore, multiple univariate indices might be used for a certain drought-type analysis, which may or may not be consistent across time. For example, SVI and SSI are both used as agricultural drought indices in multiple studies (Halwatura et al., 2015; Trenberth et al., 2014; Wang et al., 2014).

However, we observe a considerable discrepancy between them. In the 2008 forward drought, for example, SSI shows recovery to a normal and even a wet condition, whereas by 2008 SVI indicates a long period of the deficit until 2010. Such a prolonged SVI drought is attributed to vegetation stress, which could not be detected using SSI solely.

Assessing the return period of the drought plays an important role in exploring drought vulnerability and helps with long-term planning. Severity-Duration-Frequency (SDF) curves are powerful tools that display various characteristics of droughts in one plot and provide a robust risk analysis. SDF curves can be readily generated using severity, duration and frequency of historical drought occurrences with a bivariate copula model. Exploring the return periods of SVI/SWSI, SPI and SWSI, along with the $CSDI^1$/$CSDI^2$, can provide us with a new perspective relating to the performance of the $CSDI^1$/$CSDI^2$. To compute the return period levels, the severity and duration of each drought index are calculated, based on a constant threshold of -0.8 as drought onset based on method explained in Kavianpour et al. (2020). For each index, the best univariate distribution is linked to severity and duration characteristics, then the best-fitted copula to these distributions is selected, to construct their joint probability, using the MvCAT package (Sadegh et al., 2017b). Copula-provided probabilities are then translated to return period levels using an "OR" hazard analysis scenario ($RP^{\vee} = 1 / (1 - P(X \leq x \vee Y \leq y))$). The results are demonstrated in Table S6 and Fig. 10 for the SVI, SPI, SWSI and the $CSDI^1$ for the Mississippi basin at the three-month time scale. From Fig. 10 it could be noted that the return period of a drought with a duration of fewer than five months and a severity of less than five, based on the SVI, is approximately two years, which can mostly be attributed to seasonal fluctuations. The persistence of severe drought in the SWSI category exceeds SVI and the persistence of severe drought in the SVI category is greater than SPI, hence the joint realization of long durations and high severities of drought can be associated with the longest recurrence interval in SPI and SVI (lower

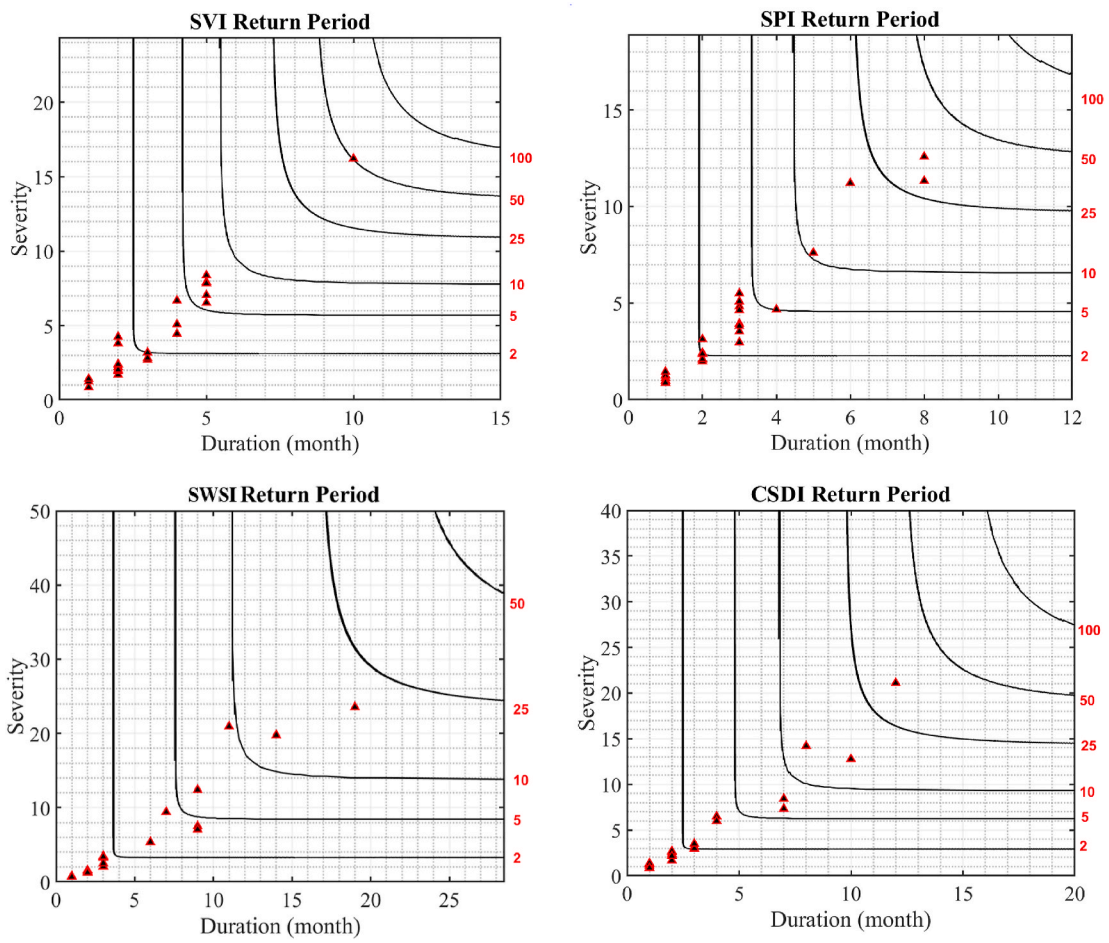

Fig. 10. SDF curves for the Mississippi basin, based on the SVI, SPI, SWSI and the $CSDI^1$. The return period years are written in a red color along the right y-axis. The red triangles indicate drought events between 1982 and 2016.

frequencies). In the case of SWSI, long and severe droughts have a shorter recurrence interval, compared to SPI and SVI, and hence are more likely to occur. As an example, for SVI and SPI, the return period of the occurrence of a drought with a duration of nine months and a severity of 15 is once in 50 years, while in the case of SWSI, a similar drought is expected to occur once in less than 10 years, on average. For a similar duration and severity at the upper level, the CSDI[1] has a higher value in terms of return period compared to SWSI and a lower value, compared to SPI, indicating that the CSDI[1] is more prone to the occurrence of droughts with longer durations and higher severities, compared with SPI, and is less prone to such droughts by comparison with SWSI. The persistence of severe drought in the SWSI category is greater than SVI, and the persistence of severe drought in the SVI category is greater than SPI, hence the joint realization of long durations and major severities of drought can have the longest recurrence interval in SPI and SVI.

In the case of CSDI[2], the persistence of drought in SSI and SWSI is also higher than SPI. The results for this case are demonstrated in Fig. 11 and Table S7. For the same duration and severity, the return period of SSI and SWSI is much higher than SPI.

For example, in the case of a drought with a severity of 10 and a duration of around eight months, the return period of occurrence for SPI is about once in every 25 years, whereas, in relation to the SSI category, the probability of the occurrence of a similar drought is once in 10 years. For SWSI, a similar drought occurs once every five years, on average, which is more likely to occur. The behavior of the CSDI[2] is most similar to SSI. For example, in the case of a drought with a duration of 20 and severity of 16, and a duration of 28 and severity of 21, the return period for the CSDI[2] is 25 and 50 years, respectively; for the SSI category, almost similar return periods are observed, while for SPI, these return period levels are more than 100 years. In the case of SWSI, the return periods for these characteristics are approximately 10 and 25 years.

4.3. Effect of ONI on global land dry–wet changes

We investigated the effects of ENSO events on ecological/agricultural, meteorological and hydrological droughts along with their joint distribution (CSDIs) using a composite analysis method. Obtaining a general overview of how these drought indices are affected by ENSO episodes can help with early drought warning systems and planning. The composite analysis is carried out, based on the method described in section 3.2 for SVI (three months), SSI (three months), SPI (three months) and SWSI (three months) over the nine strong and moderate El Niño events and five strong La Niña events during 1982–2015 and across the four seasons (JJA, SON, DJF and MAM).

In Africa (more specifically in the Nile, Niger, Okavango, Zambezi

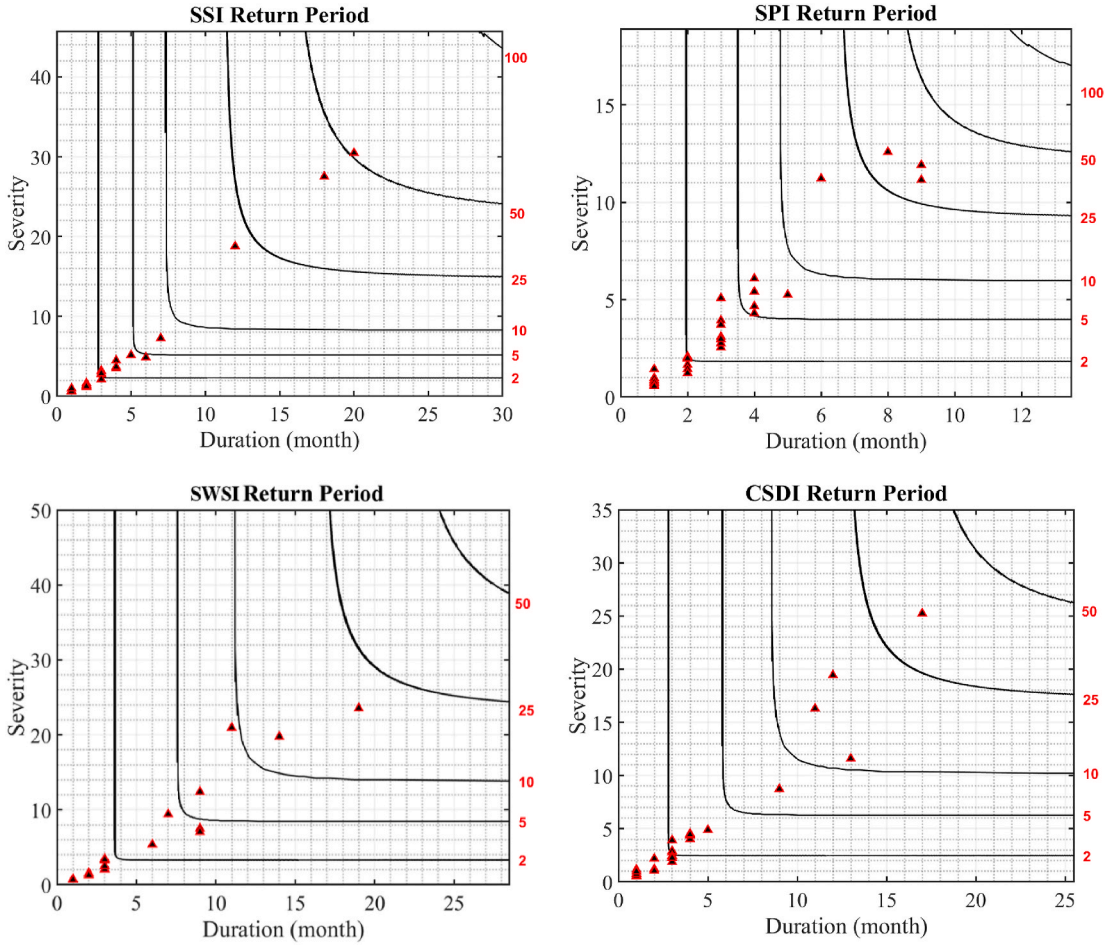

Fig. 11. SDF curves for the Mississippi basin based on the SSI, SPI, SWSI and the CSDI[2]. The return period years are written in a red color along the right y-axis. The red triangles indicate drought events between 1982 and 2016.

and Orange basins), based on the SVI, the El Niño (warm phase)-related dry–wet changes resulted in drier conditions (negative anomaly) during the SON and DJF seasons. The Mississippi, St-Lawrence, Mackenzie and Yukon basins in northern America indicated a positive anomaly in the SON and DJF seasons during El Niño events. However, in the Indus basin, El Niño induced a negative effect. During La Niña events, North America has been adversely affected in the SON and MAM seasons, especially in the Mississippi and Mackenzie basin. The Dnieper and Danube basins in Europe indicated a slight negative anomaly during the El Niño events across all seasons, while the Deniper basin indicated a significant positive anomaly during La Niña events. The impact of El Nino on basins in southern parts of Asia was mostly weak, positive during the JJA and SON seasons and negative in the DJF and MAM seasons. However, these basins demonstrated a strong positive anomaly during La Niña events in the JJA and SON seasons. In southern America, almost all the basins indicated a negative anomaly during both El Niño and La Niña events in the JJA and SON seasons. The Amazon and Parana basins demonstrated a much more significant anomaly in relation to La Niña events in the aforementioned seasons. During El Niño, the Amazon and the Tocantins basins remained negative during the DJF and MAM seasons, while Orinoco and Parana indicated a slightly positive anomaly. La Niña-induced climatic effect during DJF and MAM resulted in a significant positive anomaly for all basins in South America during the DJF and MAM seasons.

In Australia, negative anomalies during El Niño and positive anomalies during La Niña were observed. In the case of the basins located in central and northern Asia, namely Amour, Lena, Yenisei and Ob, negative anomalies of El Niño events were observed, primarily during the DJF and MAM seasons. NDVI, however, showed a delay in response to extremes in these regions as discussed by Liu et al. (2018). They identified twelve-month-persistent responses of vegetation to antecedent precipitation in central-western areas of North America and central Asia, and stated that above-ground net primary production in arid ecosystems was highly dependent on the previous years' precipitation. Huang et al. (2019) investigated the effects of ENSO events on vegetation anomalies on a global scale. Consistent with our results, they reported that the warm (cold) phase of ENSO had a positive (negative) correlation with NDVI in Russia and the United States, as well as basins located in southern Asia. Based on Fig. 12, the SSI exhibited a similar pattern with SVI in relation to the basins in North and South America, Africa, southern and northern parts of Asia, Russia and Europe but indicated a different magnitude of the anomaly. Ni et al. (2018) analyzed the correlation and phase lags between ENSO and GRACE TWS and precipitation, showing that the maximum negative correlation between TWS flux and the Niño 3.4 index occurs with a lag varying roughly between −5 and +5 months in the Amazon basin, central and northern areas of North America, southern Africa, northern and southern parts of Asia and the basins located in Australia. In the southern parts of northern and southern America, central Africa, south-west and central Asia and certain areas of East Asia, a positive correlation between TWS flux and Niño 3.4 was observed, with a lag varying between −5 and +5 and sometimes up to +10 months. A negative correlation means that El Niño has a negative effect, and a positive correlation means that El Niño has a positive effect. The SWSI composite in Fig. 13 is consistent with

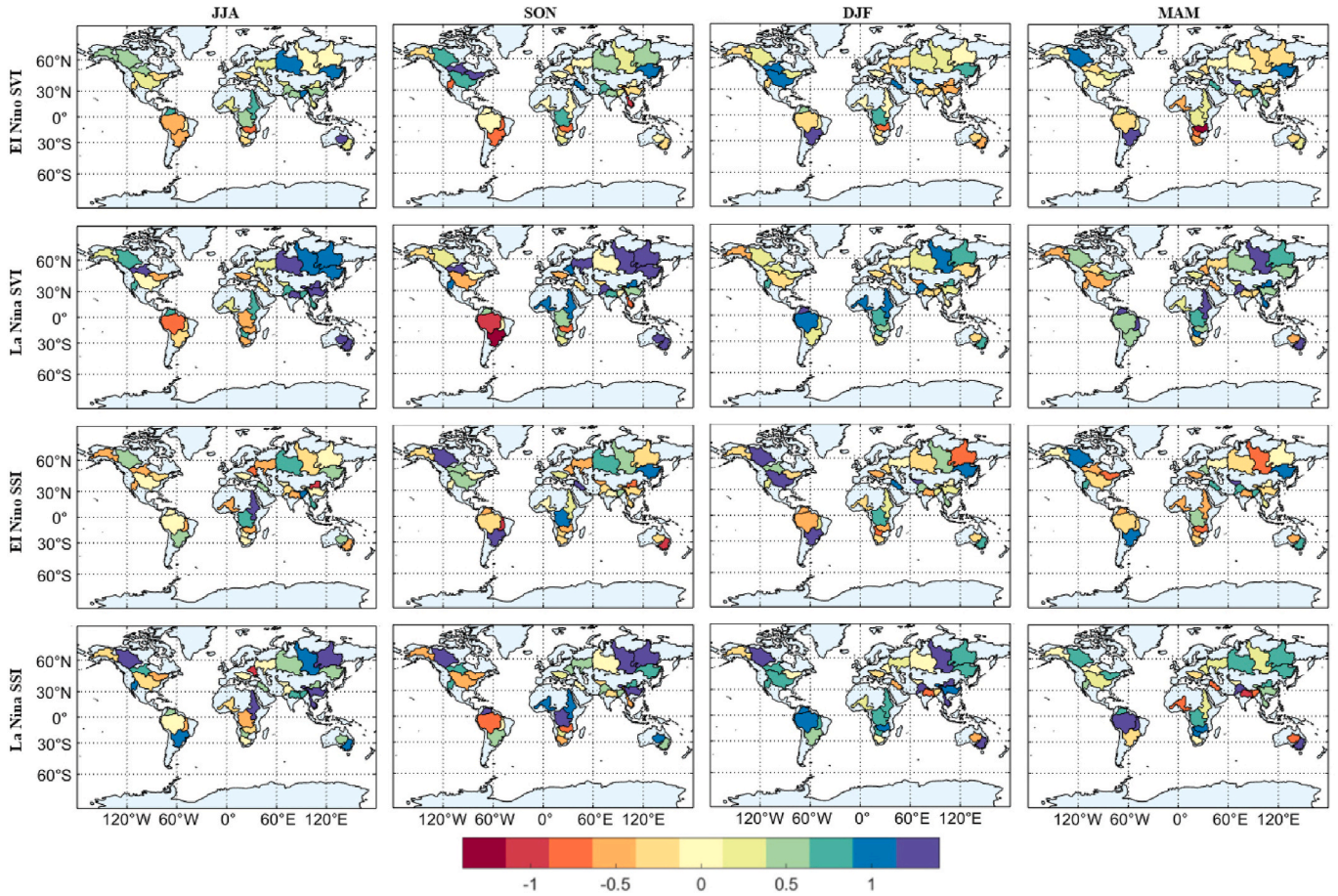

Fig. 12. Composite analysis of SVI and SSI during El Niño and La Niña events during the MAM, JJA, SON and DJF seasons. A negative value indicates a deviation from normal conditions to drought conditions and a positive value constitutes a deviation from normal to wet conditions.

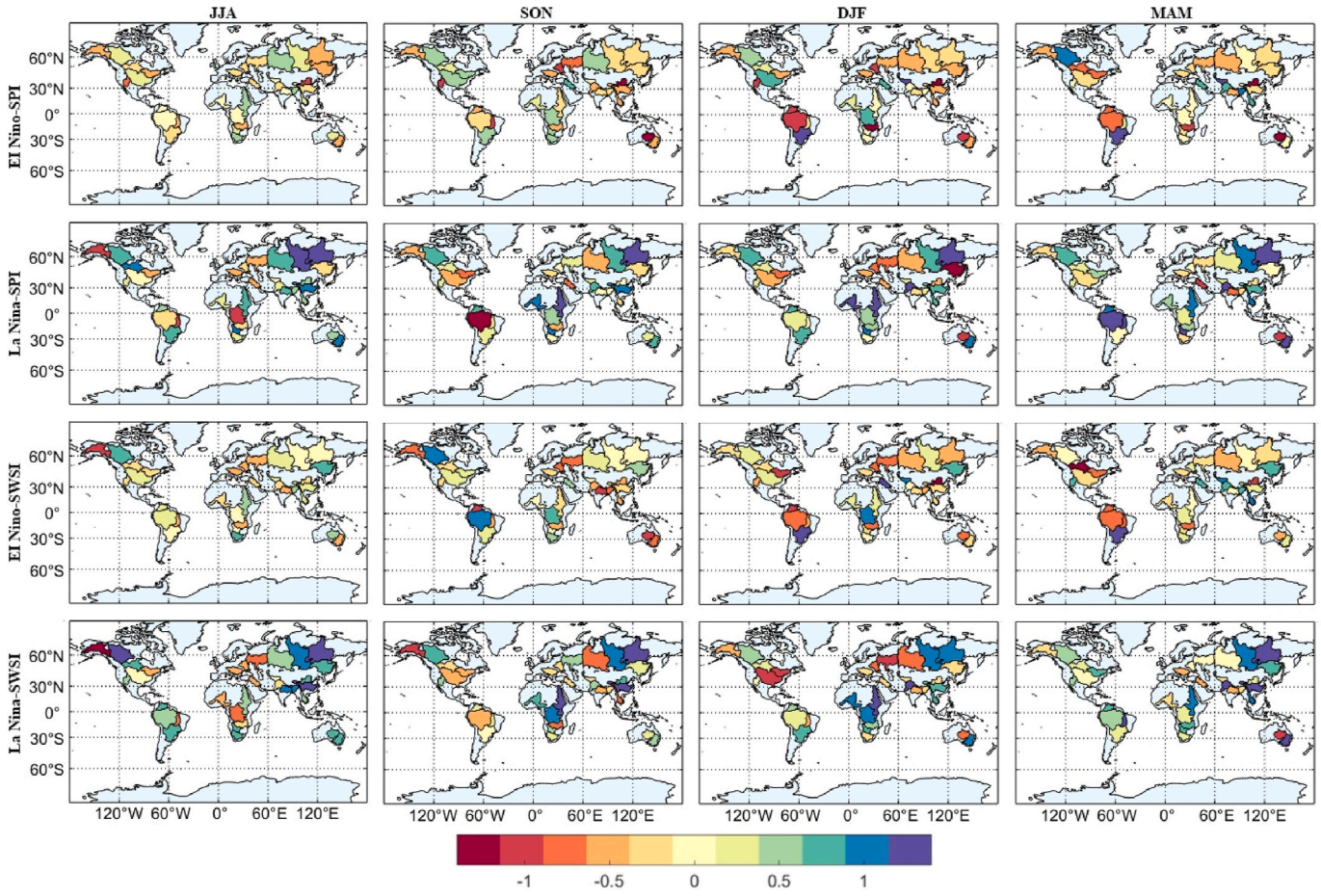

Fig. 13. A composite analysis of SPI and SWSI during El Niño and La Nina events during the MAM, JJA, SON and DJF seasons. A negative value indicates a deviation from normal conditions to drought conditions and a positive value indicates a deviation from normal to wet conditions.

these results during the SON and MAM seasons during El Niño, except in basins in North America where negative anomaly occurs with a longer lag in the MAM season. Wang et al. (2014) also investigated the effects of Pacific Decadal Oscillation and ENSO on global land dry–wet changes (based on a modified Palmer Drought Severity Index) using a composite analysis method. They reported that El Niño-related dry–wet changes resulted in drier conditions in the southern and south-eastern parts of Asia, Australia, central parts of China, northern parts of southern America and central and western areas of North America. Their results also implied that southern parts of North America, the horn of Africa, western Asia and the Mediterranean region indicated a positive anomaly.

The composite map of SPI in Fig. 13 during El Niño events conforms with their findings. Fig. 14 demonstrates the $CSDI^1$ and $CSDI^2$ composite during ENSO events. The performance of CSDIs is complex under different conditions. When all SPI and SWSI and SVI/SSI indicate negative or positive anomaly simultaneously, CSDIs also show the same anomaly. Depending on the anomaly magnitude, CSDIs generally resemble the anomaly of those univariate indices that are similar to one another. For example, in the Amazon basin, the SVI and SSI show a slightly negative anomaly (around −0.2) during El Nino events and all seasons, based on Fig. 12. According to Fig. 13 during the El Nino event, the SPI and SWSI exhibit a strong negative (around −0.9) anomaly during the DJF and MAM seasons. The $CSDI^1$ which is based on the SVI-SPI-SWSI univariate indices captures the anomaly of −0.5 during the DJF and MAM seasons. In Fig. 12 during an El Nino event, the SSI anomaly is around −0.5 in the DJF season, which is greater than the SVI anomaly in the same season (-0.2).

Accordingly, the $CSDI^2$ in Fig. 14 shows a stronger negative anomaly (-1.3) compared to the $CSDI^1$ which is −0.5. A greater negative anomaly in the SSI enables the $CSDI^2$ to capture the severity of SPI and SWSI while the lower negative anomaly of SVI mollifies the performance of the $CSDI^1$ to exhibit less severity. In the Amazon basin during La Nina events, the SVI, SSI and SPI indicate a negative anomaly during the JJA and SON seasons, followed by a significant positive anomaly in the DJF and MAM seasons. The $CSDI^1$ captures the aggregated performance of SVI, SPI and SWSI, and the $CSDI^2$ captures the aggregated performance of SSI, SPI and SWSI. The stronger positive anomaly of SSI compared to SVI, results in the $CSDI^2$ demonstrating a stronger anomaly compared to the $CSDI^1$. Carrão et al. (2016), assessed drought risk using drought hazard (based on grided precipitation deficits map), drought exposure (based on geographic layers of baseline water stress, global agricultural lands, gridded livestock and population of the world) and drought vulnerability (based on national and sub-national data of social, economic and base framework factors). They showed that geographic distribution of risk values exhibited exponential relationship with exposure and also its correlation with this determinant is stronger than hazard and vulnerability. Their presented global map of drought exposure shows that most exposed regions for drought are located in the regions such as Eastern U.S., Nigeria, India, some western regions located in

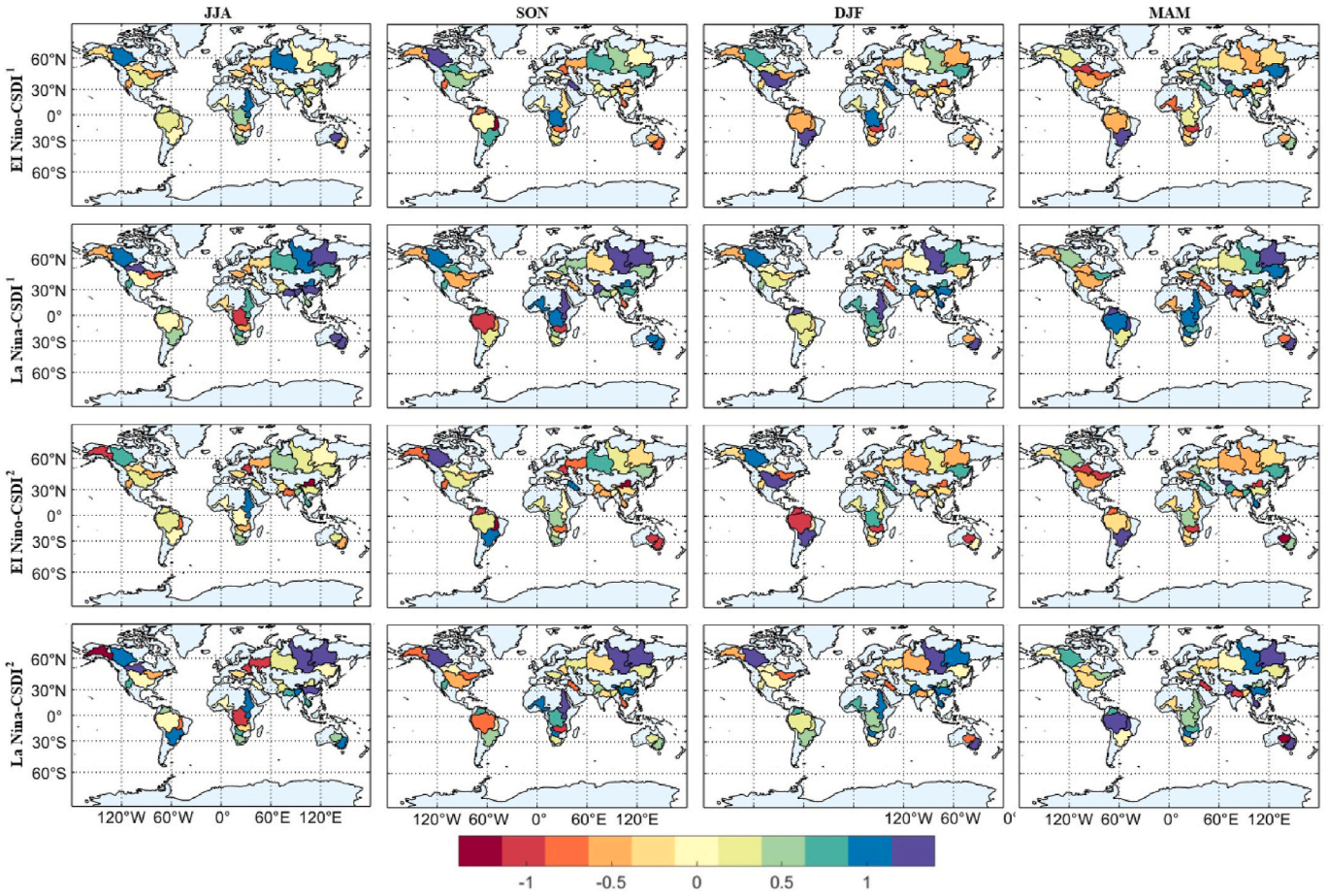

Fig. 14. Composite analysis of the $CSDI^1$ and $CSDI^2$ during El Niño and La Niña events during the JJA, SON, DJF and MAM seasons. A negative value indicates a deviation from normal conditions to drought conditions and a positive value indicates a deviation from normal to wet conditions.

South-America, south of Europe and east of China. These regions contain populated centers, agricultural and livestock activities and the lower drought exposure has been discovered in the regions like wilderness lands, tundras, and tropical forests. The $CSDI^1$ and $CSDI^2$ composite in Fig. 14 are consistent with these results during the SON and MAM seasons during La Niño, except in basins in North America where negative anomaly occurs with a longer lag in the MAM season.

To further clarify the performance of the $CSDI^1$ and $CSDI^2$, the time series of univariate and multivariate indices for the Amazon basin has been shown in Fig. 15. As is clear from Fig. 15, in 1992, SVI and SSI, which represent the ecological and agricultural indices, indicate wet conditions in the Amazon basin, while SPI and SWSI present the dry conditions. Decision-making based on SVI and SSI for agricultural purposes could be unreliable because as shown (in Fig. 15) at the end of 1992, SVI and SSI suddenly transform to dry conditions. Predicting this behavior based only on univariate indices is not possible. On the other hand, SPI and SWSI show the state of drought (dry conditions) earlier than SVI and SSI. In addition, using SPI and SWSI for management purposes is not recommended, since they capture the drought state too early. The $CSDI^1$ and $CSDI^2$ aggregate the behavior of univariate indices and transition smoothly from wet conditions to dry conditions. Therefore, CSDIs could be more reliable for drought prediction and management purposes.

Fig. 16 shows the univariate and multivariate indices for the Lena basins in Russia. As is clear from Fig. 16 b, the SSI mostly follows the overall pattern of drought and seasonal fluctuation of climatic factors that have not been captured properly. On the other hand, SPI shows a severe seasonal fluctuation. This severe fluctuation of the SPI is odd with fluctuations of SSI and SWSI. For example, in the years 1983, 1984, 1988, 1998, 2000, 2006, 2007, 2008, 2009, 2013 and 2015, SPI shows a severe anomaly, however such an anomaly is not observed in SSI and SWSI with this magnitude of severity. Making accurate decisions could be challenging in such a complicated situation, since each index exhibits different behavior. The $CSDI^2$ in Fig. 16 b shows the aggregated behavior of these univariate indices, since it follows the overall behavior of SSI and also captures the seasonal fluctuations of SPI with a lower magnitude. Based on the composite analysis in Figs. 12 and 13, SSI and SWSI during an El Nino event and during the JJA seasons, show an anomaly close to zero. SPI indicates a negative anomaly of −0.5 for the JJA season. The $CSDI^2$ demonstrated an anomaly close to zero, which reduced the effect of the SPI. Based on Fig. 16, the same behavior may be observed in other seasons in which the $CSDI^1$ and $CSDI^2$ have mollified the severe behavior of univariate indices.

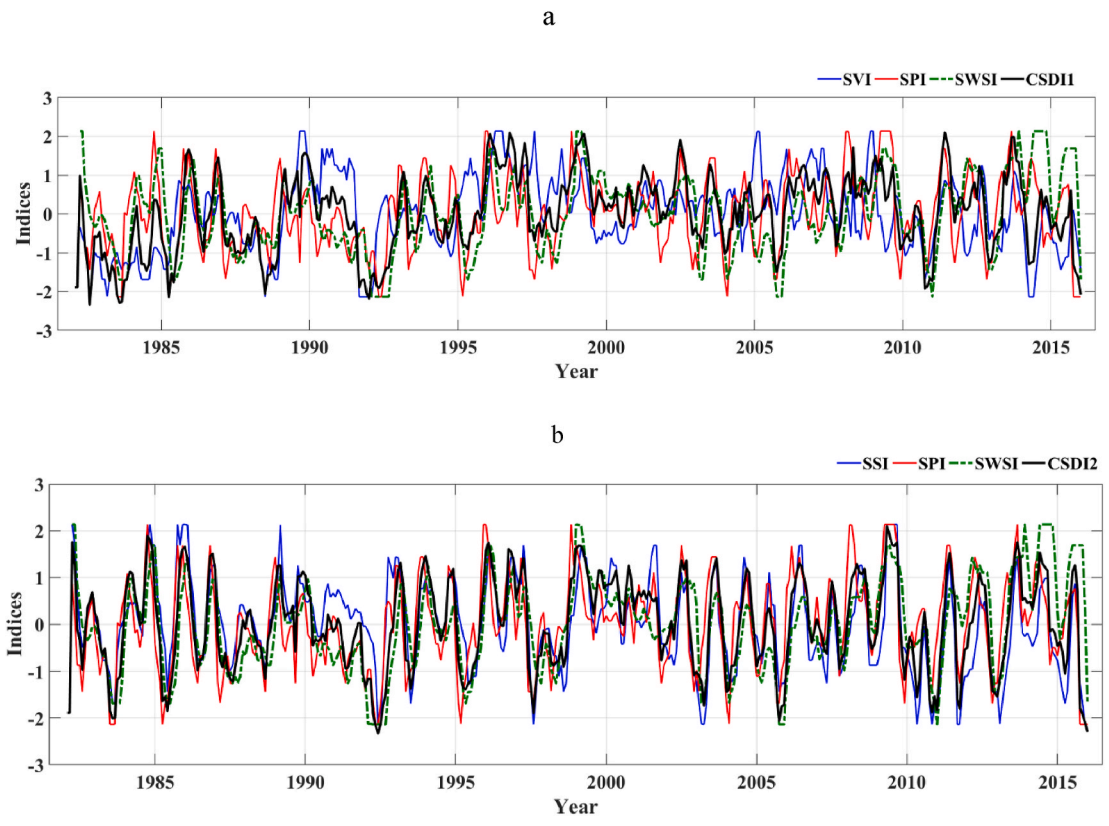

Fig. 15. Time series of a) SVI, SPI, SWSI, CSDI[1,] and b) SSI, SPI, SWSI, CSDI[2] at the three-month time scale for the Amazon basin.

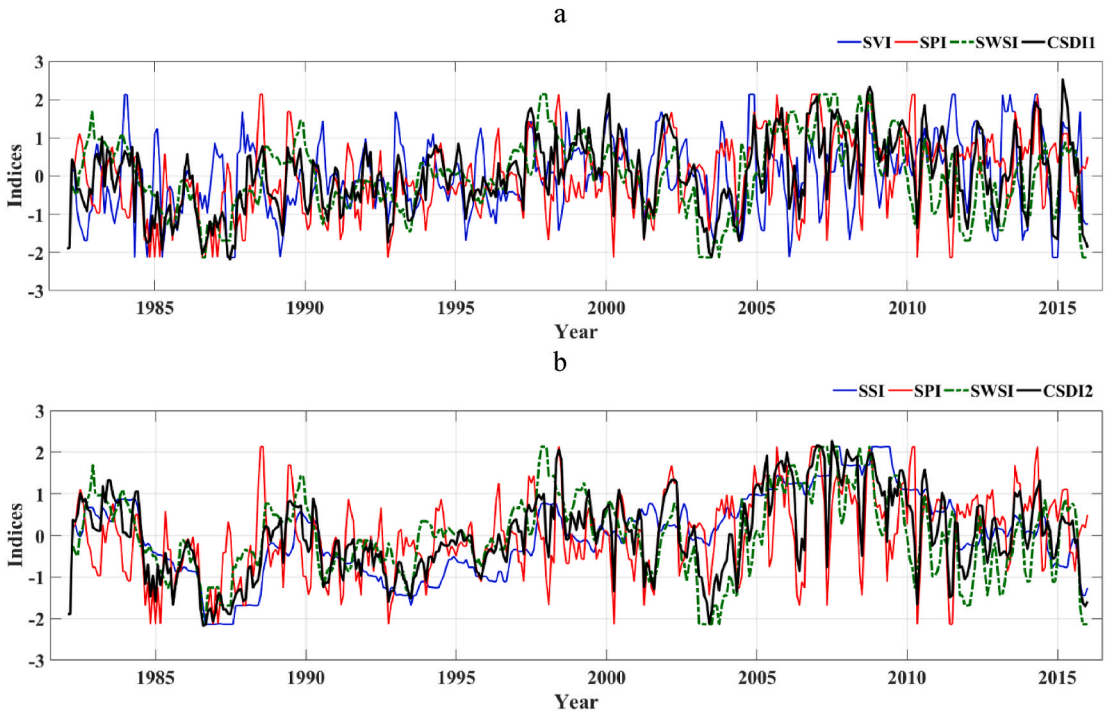

Fig. 16. Time series of a) SVI, SPI, SWSI, CSDI[1] and b) SSI, SPI, SWSI, CSDI[2] at the three-month time scale for the Lena basin.

5. Discussion

The CSDIs indices developed in this study offer novel insights for joint drought analysis by combining SPI which explains precipitation variability, SWSI which explains terrestrial water variability and SVI/SSI that represent agricultural and ecological processes.

Comparison between the theoretical and empirical probabilities of trivariate copula via statistical goodness-of-fit criteria attested to the accuracy of the fitted copula models. The results of this study indicated that using vine copula to develop a novel multivariate drought index is

effective, and the developed index better represents drought onset, development and termination than each of the univariate drought indices. Multivariate analysis of drought based on the vine copula approach evaluates Eco-meteo-hydrologic/Agri-meteo-hydrologic drought, and offers a comprehensive analysis for improved drought management. The multivariate analysis arms us with essential information proper for drought prediction and decision making (Saghafian and Sanginabadi., 2020).

Severity, duration, frequency analysis of univariate and multivariate drought indices reveals that meteorological and agricultural indices, with a certain severity and duration, have a lower recurrence interval compared to hydrological drought, implicating human intervention in drought development. Multivariate CSDIs show a higher recurrence interval compared to meteorological/agricultural droughts and a lower recurrence interval compared to the hydrological drought, which provides a balanced drought analysis incorporating human activities. Further inspection of time series of multivariate and univariate indices shows that when univariate drought indices commonly experience a severe dry or wet condition, the CSDI indices show an even more severe condition. Interestingly, when hydrological or agricultural drought indices are affected by human interventions and they show a severe condition, while the meteorological index shows a normal or wet condition, multivariate CSDI indices show a balance between the two conditions. This characteristic of multivariate indices enables a nuanced understanding of global ecosystem response to large-scale phenomena such as ENSO.

In the past few decades, many efforts have focused on developing indices for drought monitoring and analysis. These indices, however, are focused on one or a few aspects of drought, and may not provide a comprehensive enough picture of the complex natural-human system. In the past decade, a large number of studies have been using copula functions to perform multivariate frequency analysis to address various aspects of drought (Shiau, 2006; Shiau et al., 2007; Shiau and Modarres, 2009; Song and Singh, 2010; Mirabbasi et al., 2012; Chen et al., 2013; Xu et al., 2015; Montaseri et al., 2018; Mortuza et al., 2019; Nabaei et al., 2019). Our study builds upon this literature and develops a trivariate drought index (Svoboda et al., 2002; Kao and Govindaraju, 2010a,b; Xia et al., 2014a, 2014b; Vazifehkhah et al., 2019; Wang et al., 2019). A unique aspect of the herein proposed drought indices is including proxies for human-induced changes in the basin-scale water availability and distribution, resulting in indices that better capture the state of drought and offer greater predictability from large-scale climate anomalies.

Since drought propagation (transform from metrological drought to hydrological or agricultural drought) time lag and effect of anthropogenic activities on hydro-agricultural drought varies in different region of the glob, analyzing the effect of ENSO on global ecosystem using univariate indices would be challenging, while by using these new multivariate indices we will be able to address these factors more comprehensively. Our novel multivariate indices outperformed the univariate indices performance and they show to improve the drought quantification, which could be used for management purposes and guidance. The major limitation of this study is that we have not performed uncertainty analysis for our results. This would be our objective for future work and also, the anthropogenic impact on drought should be more highlighted and the performance of multivariate indices in detecting anthropogenic drought.

6. Conclusions

Droughts can be characterized based on different hydrological, meteorological, agricultural and ecological variables, each representing certain aspects of this complex phenomenon. Univariate drought indices have traditionally been used to inform drought management; however, studies have shown that multivariate indices are better poised to capture various characteristics of this complex phenomenon. This study offers improved understanding of drought teleconnections, as represented through multivariate indices that capture impacts on multiple sectors, through which the managers can better prepare for drought mitigation. In this study, we employed Vine copula to develop two new, probabilistic, multivariate drought indices (ecological-meteorological-hydrological and agricultural-meteorological-hydrological) by combining data from TWS, soil moisture, precipitation and NDVI. Furthermore, we used these indices to evaluate the impact of ENSO on drought conditions across various major river basins around the globe. We estimated these indices for 33 major river basins globally between the period 1982 to 2015, each reflecting the drought evolution based on the state of multiple drought variables. Theoretical and empirical probability distribution functions of these drought indices are compared, to evaluate the robustness of inferences regarding two versions of a multivariate CSDI, ($CSDI^1$ and $CSDI^2$). We then compared the return periods of drought duration and the severity of CSDIs with those hydrological, meteorological, agricultural and ecological drought indices. Finally, we applied a composite analysis to assess the impact of ENSO on drought onset, severity, and termination on a global scale. The novelties of this study includes:

- A nuanced, improved understanding of the impacts of univariate index selection on multivariate drought analysis within the vine copula modeling framework
- Incorporation of the impacts of anthropogenic activities in drought analysis, using irrigation-induced soil moisture proxy, and development of trivariate drought indices that improve ecological and agricultural drought analysis.
- Improved understanding of teleconnection impacts on drought onset, development and termination, as demonstrated through a composite analysis of El Nino and La Nina phenomena and multivariate drought indices.
- Comprehensive investigation of the performance of multivariate indices in capturing the effect of ENSO on global ecosystem response as compared to univariate indices.

In summary, we conclude:

- the combination of Archimedean and Elliptical copulas is more effective in developing Vine copula trees by comparison with using one of these copula families.
- comparing empirical and theoretical PDFs shows that the constructed Vine copula can simulate the three-dimensional joint distribution very well.
- multivariate drought indices capture the state of multiple drought indices. Hence, drought duration and intensity, based on CSDI, is an integrated representation of the univariate drought indices.
- CSDI reveals a more comprehensive picture of intensity, duration and frequency of droughts, compared to univariate indices. In general, SPI and SVI/SSI with a different severity and duration have a lower recurrence interval, compared to SWSI. CSDI, in the case of a common drought, shows a higher recurrence interval compared to SPI and SVI/SSI and a lower recurrence interval compared to SWSI. This implies that CSDI maintains a balance between different drought indices.
- The impacts of El Niño and La Niña events on regional drought occurrences are significant around the globe, and the impact is similar for different drought indices. These impacts are observed mostly in the fall (SON months) in the majority of the basins studied. A composite analysis, based on the CSDI, can extract more conclusive anomalies than univariate indices, as the CSDI analyzes a more comprehensive representation of the ecosystem response to teleconnections.

Overall, we conclude that the application of the Vine copula approach to developing a multivariate drought index, using agricultural,

meteorological, hydrological and ecological indices, results in a statistically representative drought index. The combined drought indices developed in this study indicated an improvement in detecting the relationship between teleconnections and drought on a global scale.

Funding

This work was financially supported by the Centre for Advanced Modelling and Geospatial Information Systems (CAMGIS), Faculty of Engineering and IT, University of Technology Sydney (UTS).

Author statement

Zahir Nikrfatar: Conceptualization, Methodology, Modelling, Visualization, Writing original draft, Abdorrahman Mostafaie: Conceptualization, Methodology, Writing original draft, Mojtaba Sadegh: Technical guidance, Validation, Review & Editing, Supervision, Javad Hatami Afkueieh: Modelling, Review & Editing, Biswajeet Pradhan: Review & Editing, Supervision, Resources, Funding.

Declaration of competing interest

The authors declare that they have no known competing financial interests or personal relationships that could have appeared to influence the work reported in this paper.

Appendix: abbreviation lists

Abbreviation	
CSDI	Combined Standardized Drought Index
JDI	Joint Deficit Index
SPI	Standardized Precipitation Index
SSI	Standardized Soil Moisture Index
MSDI	Multivariate Standardized Drought Index
SRI	Standard Runoff Index
NMDI	Nonlinear Multivariate Drought Index
SDI	Standardized Drought Index
CDI	Combined Drought Index
SWSI	Standardized Water Storage Index
SVI	Standardized Vegetation Index
ENSO	El Ni ñ o Southern Oscillation
TWS	Terrestrial Water Storage
GIA	Glacial Isostatic Adjustment
MERRA	Modern-Era Retrospective analysis for Research and Applications
NDVI	Normalized Difference Vegetation Index
AVHRR	Advanced Very High-Resolution Radiometer
FEWS	Famine and Early Warning System
GIMMS	Global Inventory Monitoring and Modeling System
WMO	World Meteorological Organization
SDAT	Standardized Drought Analysis Toolbox
CDF	Cumulative Distribution Function
K-S	Kolmogorov-Smirnov
CvM	Cramr-Von Mises
SDF	Severity-Duration-Frequency
SPDI-JDI	Standardized Palmer Drought Index-based Joint Drought Index

Appendix A. Supplementary data

Supplementary data to this article can be found online at https://doi.org/10.1016/j.wace.2021.100402.

References

Abdi, A., Hassanzadeh, Y., Ouarda, T.B.M.J., 2017. Regional frequency analysis using Growing Neural Gas network. J. Hydrol. https://doi.org/10.1016/j.jhydrol.2017.04.047.

AghaKouchak, A., 2014. A baseline probabilistic drought forecasting framework using standardized soil moisture index: application to the 2012 United States drought. Hydrol. Earth Syst. Sci. https://doi.org/10.5194/hess-18-2485-2014.

Aghakouchak, A., Nakhjiri, N., 2012. A near real-time satellite-based global drought climate data record. Environ. Res. Lett. https://doi.org/10.1088/1748-9326/7/4/044037.

American Meteorological Society AMS, 2004. Statement on meteorological drought. Bull. Am. Meteorol. Soc. 85, 771–773.

Balint, Z., Mutua, F., Muchiri, P., Omuto, C.T., 2013. Monitoring drought with the combined drought index in Kenya. In: Developments in Earth Surface Processes. https://doi.org/10.1016/B978-0-444-59559-1.00023-2.

Bayissa, Y., Maskey, S., Tadesse, T., van Andel, S.J., Moges, S., van Griensven, A., Solomatine, D., 2018. Comparison of the performance of six drought indices in characterizing historical drought for the upper Blue Nile Basin, Ethiopia. Geoscience. https://doi.org/10.3390/geosciences8030081.

Bazrafshan, J., Hejabi, S., Rahimi, J., 2014. Drought monitoring using the multivariate standardized precipitation index (MSPI). Water resour. Manag. https://doi.org/10.1007/s11269-014-0533-2.

Bazrafshan, J., Nadi, M., Ghorbani, K., 2015. Comparison of Empirical Copula-Based Joint Deficit Index (JDI) and Multivariate Standardized Precipitation Index (MSPI) for Drought Monitoring in Iran. Water Resour. Manag. https://doi.org/10.1007/s11269-015-0926-x.

Carrão, H., Naumann, G., Barbosa, P., 2016. Mapping global patterns of drought risk: an empirical framework based on sub-national estimates of hazard, exposure and vulnerability. Global Environ. Change 39, 108–124. https://doi.org/10.1016/j.gloenvcha.2016.04.012.

Chang, J., Li, Y., Wang, Y., Yuan, M., 2016. Copula-based drought risk assessment combined with an integrated index in the Wei River Basin, China. J. Hydrol. https://doi.org/10.1016/j.jhydrol.2016.06.064.

Chen, J.L., Wilson, C.R., Tapley, B.D., Grand, S., 2007. GRACE detects coseismic and postseismic deformation from the Sumatra-Andaman earthquake. Geophys. Res. Lett. 34 (13) https://doi.org/10.1029/2007GL030356.
Chen, L., Singh, V.P., Guo, S., Mishra, A.K., Guo, J., 2013. Drought analysis using copulas. J. Hydrol. Eng. 18 (7), 797–808. https://doi.org/10.1061/(ASCE)HE.1943-5584.0000697.
Dai, A., Wigley, T.M.L., 2000. Global patterns of ENSO-induced precipitation. Geophys. Res. Lett. https://doi.org/10.1029/1999GL011140.
Davey, M.K., Brookshaw, A., Ineson, S., 2014. The probability of the impact of ENSO on precipitation and near-surface temperature. Clim. Risk Manag. https://doi.org/10.1016/j.crm.2013.12.002.
Dikshit, A., Pradhan, B., 2021. Interpretable and explainable AI (XAI) model for spatial drought prediction. Sci. Total Environ. 801, 149797.
Dikshit, A., Pradhan, B., Alamri, A.M., 2020a. Pathways and challenges of the application of artificial intelligence to geohazards modelling. Gondwana Res. https://doi.org/10.1016/j.gr.2020.08.007.
Dikshit, A., Pradhan, B., Alamri, A.M., 2020b. Temporal hydrological drought index forecasting for New South Wales, Australia using machine learning approaches. Atmosphere 11, 585.
Dikshit, A., Pradhan, B., Alamri, A.M., 2021a. Long lead time drought forecasting using lagged climate variables and a stacked long short-term memory model. Sci. Total Environ. 755, 142638.
Dikshit, A., Pradhan, B., Huete, A., 2021b. An improved SPEI drought forecasting approach using the long short-term memory neural network. J. Environ. Manag. 283, 111979.
Farahmand, A., AghaKouchak, A., 2015. A generalized framework for deriving nonparametric standardized drought indicators. Adv. Water Resour. https://doi.org/10.1016/j.advwatres.2014.11.012.
Forootan, E., Khaki, M., Schumacher, M., Wulfmeyer, V., Mehrnegar, N., van Dijk, A.I.J. M., Brocca, L., Farzaneh, S., Akinluyi, F., Ramillien, G., Shum, C.K., Awange, J., Mostafaie, A., 2019. Understanding the global hydrological droughts of 2003–2016 and their relationships with teleconnections. Sci. Total Environ. https://doi.org/10.1016/j.scitotenv.2018.09.231.
Gringorten, I.I., 1963. A plotting rule for extreme probability paper. J. Geophys. Res. https://doi.org/10.1029/jz068i003p00813.
Halwatura, D., Lechner, A.M., Arnold, S., 2015. Drought severity-duration-frequency curves: a foundation for risk assessment and planning tool for ecosystem establishment in post-mining landscapes. Hydrol. Earth Syst. Sci. https://doi.org/10.5194/hess-19-1069-2015.
Hao, Z., AghaKouchak, A., 2013. Multivariate standardized drought index: a parametric multi-index model. Adv. Water Resour. https://doi.org/10.1016/j.advwatres.2013.03.009.
Harisuseno, D., 2020. Meteorological drought and its relationship with southern oscillation index (SOI). Civil Eng. J. 6 (10), 1864–1875. https://doi.org/10.28991/cej-2020-03091588.
Huang, M., Wang, Z., Wang, S., Gu, F., Gong, H., Hao, M., Shao, Y., 2019. Global vegetation productivity responses to the west Pacific warm Pool. Sci. Total Environ. https://doi.org/10.1016/j.scitotenv.2018.11.170.
Jiao, W., Tian, C., Chang, Q., Novick, K.A., Wang, L., 2019. A new multi-sensor integrated index for drought monitoring. Agricultural and Forest Meteorology. https://doi.org/10.1016/j.agrformet.2019.01.008.
Kao, S.C., Govindaraju, R.S., 2010a. A copula-based joint deficit index for droughts. J. Hydrol. https://doi.org/10.1016/j.jhydrol.2009.10.029.
Kao, S.C., Govindaraju, R.S., 2010b. A copula-based joint deficit index for droughts. J. Hydrol. 380 (1–2), 121–134. https://doi.org/10.1016/j.jhydrol.2009.10.029.
Kavianpour, M., Seyedabadi, M., Moazami, S., 2018. Spatial and temporal analysis of drought based on a combined index using copula. Environ. Earth Sci. https://doi.org/10.1007/s12665-018-7942-0.
Kavianpour, M., Seyedabadi, M., Moazami, S., Yamini, O.A., 2020. Copula based spatial analysis of drought return period in Southwest of Iran. Period. Polytech. Civ. Eng. 64 (4), 1051–1063. https://doi.org/10.3311/PPci.16301.
Keyantash, J.A., Dracup, J.A., 2004. An aggregate drought index: assessing drought severity based on fluctuations in the hydrologic cycle and surface water storage. Water Resour. Res. https://doi.org/10.1029/2003WR002610.
Kiladis, G.N., Diaz, H.F., 1989. Global climatic anomalies associated with extremes in the southern oscillation. J. Clim. 2 https://doi.org/10.1175/1520-0442(1989)002<1069:gcaawe>2.0.co.
Kusche, J., Schmidt, R., Petrovic, S., Rietbroek, R., 2009. Decorrelated GRACE time-variable gravity solutions by GFZ, and their validation using a hydrological model. J. Geodyn. https://doi.org/10.1007/s00190-009-0308-3.
Liu, L., Zhang, Y., Wu, S., Li, S., Qin, D., 2018. Water memory effects and their impacts on global vegetation productivity and resilience. Sci. Rep. https://doi.org/10.1038/s41598-018-21339-4.
Ma, M., Ren, L., Singh, V.P., Tu, X., Jiang, S., Liu, Y., 2015. Evaluation and application of the SPDI-JDI for droughts in Texas, USA. J. Hydrol. https://doi.org/10.1016/j.jhydrol.2014.11.074.
McKee, T.B., Doesken, N.J., Kleist, J., 1993. The relationship of drought frequency and duration to time scales. In: Proceedings of the 8th Conference on Applied Climatology, pp. 179–183.
Mellak, S., Souag-Gamane, D., 2020. Spatio-temporal analysis of maximum drought severity using Copulas in Northern Algeria. J. Water Clim. Chang. https://doi.org/10.2166/wcc.2020.070.
Mirabbasi, R., Fakheri-Fard, A., Dinpashoh, Y., 2012. Bivariate drought frequency analysis using the copula method. Theor. Appl. Climatol. 108 (1), 191–206. https://doi.org/10.1007/s00704-011-0524-7.
Mirabbasi, R., Anagnostou, E.N., Fakheri-Fard, A., Dinpashoh, Y., Eslamian, S., 2013. Analysis of meteorological drought in northwest Iran using the Joint Deficit Index. J. Hydrol. https://doi.org/10.1016/j.jhydrol.2013.04.019.
Montaseri, M., Amirataee, B., Rezaie, H., 2018. New approach in bivariate drought duration and severity analysis. J. Hydrol. 559, 166–181. https://doi.org/10.1016/j.jhydrol.2018.02.018.
Mortuza, M.R., Moges, E., Demissie, Y., Li, H.Y., 2019. Historical and future drought in Bangladesh using copula-based bivariate regional frequency analysis. Theor. Appl. Climatol. 135 (3), 855–871. https://doi.org/10.1007/s00704-018-2407-7.
Murthy, C.S., Singh, J., Kumar, P., Sesha Sai, M.V.R., 2017. A composite index for drought hazard assessment using CPC rainfall time series data. Int. J. Environ. Sci. Technol. https://doi.org/10.1007/s13762-017-1278-2.
Nabaei, S., Sharafati, A., Yaseen, Z.M., Shahid, S., 2019. Copula based assessment of meteorological drought characteristics: regional investigation of Iran. Agric. For. Meteorol. 276–277, 107611 https://doi.org/10.1016/j.agrformet.2019.06.010.
Ni, S., Chen, J., Wilson, C.R., Li, J., Hu, X., Fu, R., 2018. Global terrestrial water storage changes and connections to ENSO events. Surv. Geophys. https://doi.org/10.1007/s10712-017-9421-7.
Rad, A.M., Ghahraman, B., Khalili, D., Ghahremani, Z., Ardakani, S.A., 2017. Integrated meteorological and hydrological drought model: a management tool for proactive water resources planning of semi-arid regions. Adv. Water Resour. https://doi.org/10.1016/j.advwatres.2017.07.007.
Rajsekhar, D., Singh, V.P., Mishra, A.K., 2015. Multivariate drought index: an information theory based approach for integrated drought assessment. J. Hydrol. https://doi.org/10.1016/j.jhydrol.2014.11.031.
Rienecker, M.M., Suarez, M.J., Gelaro, R., Todling, R., Bacmeister, J., Liu, E., Bosilovich, M.G., Schubert, S.D., Takacs, L., Kim, G.K., Bloom, S., Chen, J., Collins, D., Conaty, A., Da Silva, A., Gu, W., Joiner, J., Koster, R.D., Lucchesi, R., Molod, A., Owens, T., Pawson, S., Pegion, P., Redder, C.R., Reichle, R., Robertson, F. R., Ruddick, A.G., Sienkiewicz, M., Woollen, J., 2011. MERRA: NASA's modern-era retrospective analysis for research and applications. J. Clim. https://doi.org/10.1175/JCLI-D-11-00015.1.
Ropelewski, C.F., Halpert, M.S., 1987. Global and regional scale precipitation patterns associated with the El Niño/southern oscillation. Mon. Weather Rev. https://doi.org/10.1175/1520-0493(1987)115<1606:garspp>2.0.co;2.
Rouse Jr., J.W., Haas, R.H., Schell, J.A., Deering, D.W., 1974. Monitoring vegetation systems in the great plains with erts. In: NASA SP-351, 3rd ERTS-1 Symposium.
Sadegh, M., Love, C., Farahmand, A., Mehran, A., Tourian, M.J., AghaKouchak, A., 2017a. Multi-Sensor Remote Sensing of Drought from Space. https://doi.org/10.1007/978-3-319-43744-6_11.
Sadegh, Mojtaba, Ragno, E., AghaKouchak, A., 2017b. Multivariate copula analysis Toolbox (MvCAT): describing dependence and underlying uncertainty using a Bayesian framework. Water Resour. Res. https://doi.org/10.1002/2016WR020242.
Sadegh, M., Moftakhari, H., Gupta, H.V., Ragno, E., Mazdiyasni, O., Sanders, B., Matthew, R., AghaKouchak, A., 2018. Multihazard scenarios for analysis of compound extreme events. Geophys. Res. Lett. https://doi.org/10.1029/2018GL077317.
Saghafian, B., Sanginabadi, H., 2020. Multivariate groundwater drought analysis using copulas. Hydrol. Res. 51 (4), 666–685. https://doi.org/10.2166/nh.2020.131.
Schepsmeier, U., Stoeber, J., Brechmann, E.C., Graeler, B., Nagler, T., Erhardt, T., et al., 2018. Package 'VineCopula. R Pack. Vers. 2 (5).
Shiau, J.T., 2006. Fitting drought duration and severity with two-dimensional copulas. Water Resour. Manag. 20 (5), 795–815. https://doi.org/10.1007/s11269-005-9008-9.
Shiau, J.T., Modarres, R., 2009. Copula-based drought severity-duration-frequency analysis in Iran. Meteorol. Appl.: J. Forecast., Pract. Appl., Train. Techn. Model. 16 (4), 481–489. https://doi.org/10.1002/met.145.
Shiau, J.T., Feng, S., Nadarajah, S., 2007. Assessment of hydrological droughts for the Yellow River, China, using copulas. Hydrol. Process.: Int. J. 21 (16), 2157–2163. https://doi.org/10.1002/hyp.6400.
Sklar, A., 1959. Fonctions de R{é}partition {à} n Dimensions et Leurs Marges. Publ. L'Institut. Stat. L'Univ. Paris.
Song, S., Singh, V.P., 2010. Meta-elliptical copulas for drought frequency analysis of periodic hydrologic data. Stoch. Environ. Res. Risk Assess. 24 (3), 425–444. https://doi.org/10.1007/s00477-009-0331-1.
Svoboda, M., LeComte, D., Hayes, M., Heim, R., Gleason, K., Angel, J., Rippey, B., Tinker, R., Palecki, M., Stooksbury, D., Miskus, D., 2002. The drought monitor. Bull. Am. Meteorol. Soc. 83 (8), 1181–1190. https://doi.org/10.1175/1520-0477-83.8.1181.
Swenson, S., Chambers, D., Wahr, J., 2008. Estimating geocenter variations from a combination of GRACE and ocean model output. J. Geophys. Res.: Solid Earth 113 (B8). https://doi.org/10.1029/2007JB005338.
Tamaddun, K.A., Kalra, A., Bernardez, M., Ahmad, S., 2019. Effects of ENSO on Temperature, Precipitation, and Potential Evapotranspiration of North India's Monsoon: an Analysis of Trend and Entropy. Water, Switzerland. https://doi.org/10.3390/w11020189.
Trenberth, K.E., Branstator, G.W., Karoly, D., Kumar, A., Lau, N.-C., Ropelewski, C., 1998. Progress during TOGA in understanding and modeling global teleconnections associated with tropical sea surface temperatures. J. Geophys. Res. Ocean. https://doi.org/10.1029/97jc01444.
Trenberth, K.E., Dai, A., Van Der Schrier, G., Jones, P.D., Barichivich, J., Briffa, K.R., Sheffield, J., 2014. Global warming and changes in drought. Nat. Clim. Change. https://doi.org/10.1038/nclimate2067.
Tucker, C.J., Pinzon, J.E., Brown, M.E., Slayback, D.A., Pak, E.W., Mahoney, R., Vermote, E.F., El Saleous, N., 2005. An extended AVHRR 8-km NDVI dataset

compatible with MODIS and SPOT vegetation NDVI data. Int. J. Rem. Sens. https://doi.org/10.1080/01431160500168686.
van Dijk, A.I.J.M., 2010. The Australian Water Resources Assessment System: Technical Report 3. Landscape Model (Version 0.5) Technical Description. WIRADA/CSIRO Water a Heal. Ctry. Flagship, Canberra. https://doi.org/10.1117/12.776881.
Vazifehkhah, S., Tosunoglu, F., Kahya, E., 2019. Bivariate risk analysis of droughts using a nonparametric multivariate standardized drought index and copulas. J. Hydrol. Eng. 24 (5), 5019006 https://doi.org/10.1061/(ASCE)HE.1943-5584.0001775.
Wahr, J., Molenaar, M., Bryan, F., 1998. Time variability of the Earth's gravity field: hydrological and oceanic effects and their possible detection using GRACE. J. Geophys. Res. Solid Earth. https://doi.org/10.1029/98jb02844.
Wang, S., Huang, J., He, Y., Guan, Y., 2014. Combined effects of the Pacific decadal oscillation and El Niño-southern oscillation on global land dry-wet changes. Sci. Rep. https://doi.org/10.1038/srep06651.
Wang, H., Chen, Y., Pan, Y., Chen, Z., Ren, Z., 2019. Assessment of candidate distributions for SPI/SPEI and sensitivity of drought to climatic variables in China. Int. J. Climatol. 39 (11), 4392–4412. https://doi.org/10.1002/joc.6081.
Waseem, M., Ajmal, M., Kim, T.W., 2015. Development of a new composite drought index for multivariate drought assessment. J. Hydrol. https://doi.org/10.1016/j.jhydrol.2015.04.044.
Wilhite, D.A., Glantz, M.H., 1985. Understanding: the drought phenomenon: the role of definitions. Water Int. https://doi.org/10.1080/02508068508686328.
Xia, Y., Ek, M.B., Mocko, D., Peters-Lidard, C.D., Sheffield, J., Dong, J., Wood, E.F., 2014a. Uncertainties, correlations, and optimal blends of drought indices from the NLDAS multiple land surface model ensemble. J. Hydrometeorol. 15 (4), 1636–1650. https://doi.org/10.1175/JHM-D-13-058.1.
Xia, Y., Ek, M.B., Peters-Lidard, C.D., Mocko, D., Svoboda, M., Sheffield, J., Wood, E.F., 2014b. Application of USDM statistics in NLDAS-2: optimal blended NLDAS drought index over the continental United States. J. Geophys. Res.: Atmos. 119 (6), 2947–2965. https://doi.org/10.1002/2013JD020994.
Xu, K., Yang, D., Xu, X., Lei, H., 2015. Copula based drought frequency analysis considering the spatio-temporal variability in Southwest China. J. Hydrol. 527, 630–640. https://doi.org/10.1016/j.jhydrol.2015.05.030.
Yang, X., Delsole, T., 2012. Systematic comparison of enso teleconnection patterns between models and observations. J. Clim. https://doi.org/10.1175/JCLI-D-11-00175.1.
Yang, J., Chang, J., Wang, Y., Li, Y., Hu, H., Chen, Y., Huang, Q., Yao, J., 2018. Comprehensive drought characteristics analysis based on a nonlinear multivariate drought index. J. Hydrol. https://doi.org/10.1016/j.jhydrol.2017.12.055.
Yeh, S.W., Cai, W., Min, S.K., McPhaden, M.J., Dommenget, D., Dewitte, B., Collins, M., Ashok, K., An, S. Il, Yim, B.Y., Kug, J.S., 2018. ENSO atmospheric teleconnections and their response to greenhouse gas forcing. Rev. Geophys. https://doi.org/10.1002/2017RG000568.
Zargar, A., Sadiq, R., Naser, B., Khan, F.I., 2011. A review of drought indices. Environ. Rev. https://doi.org/10.1139/a11-013.
Zhang, D., Chen, P., Zhang, Q., Li, X., 2017. Copula-based probability of concurrent hydrological drought in the Poyang lake-catchment-river system (China) from 1960 to 2013. J. Hydrol. https://doi.org/10.1016/j.jhydrol.2017.08.046.
Zhu, N., Xu, J., Li, W., Li, K., Zhou, C., 2018. A comprehensive approach to assess the hydrological drought of inland river basin in Northwest China. Atmosphere. https://doi.org/10.3390/atmos9100.